



The Unconventional Cytoplasmic Sensing Mechanism for Ethanol Chemotaxis in *Bacillus subtilis*

Payman Tohidifar,^a Girija A. Bodhankar,^a Sichong Pei,^a C. Keith Cassidy,^c Hanna E. Walukiewicz,^{a,b} George W. Ordal,^b Phillip J. Stansfeld,^{d,e}  Christopher V. Rao^a

^aDepartment of Chemical and Biomolecular Engineering, University of Illinois at Urbana-Champaign, Urbana, Illinois, USA

^bDepartment of Biochemistry, University of Illinois at Urbana-Champaign, Urbana, Illinois, USA

^cDepartment of Biochemistry, University of Oxford, Oxford, United Kingdom

^dSchool of Life Sciences, University of Warwick, Coventry, United Kingdom

^eDepartment of Chemistry, University of Warwick, Coventry, United Kingdom

Payman Tohidifar, Girija A. Bodhankar, and Sichong Pei contributed equally to this work. Author order was determined on the basis of seniority.

ABSTRACT Motile bacteria sense chemical gradients using chemoreceptors, which consist of distinct sensing and signaling domains. The general model is that the sensing domain binds the chemical and the signaling domain induces the tactic response. Here, we investigated the unconventional sensing mechanism for ethanol taxis in *Bacillus subtilis*. Ethanol and other short-chain alcohols are attractants for *B. subtilis*. Two chemoreceptors, McpB and HemAT, sense these alcohols. In the case of McpB, the signaling domain directly binds ethanol. We were further able to identify a single amino acid residue, Ala⁴³¹, on the cytoplasmic signaling domain of McpB that, when mutated to serine, reduces taxis to alcohols. Molecular dynamics simulations suggest that the conversion of Ala⁴³¹ to serine increases coiled-coil packing within the signaling domain, thereby reducing the ability of ethanol to bind between the helices of the signaling domain. In the case of HemAT, the myoglobin-like sensing domain binds ethanol, likely between the helices encapsulating the heme group. Aside from being sensed by an unconventional mechanism, ethanol also differs from many other chemoattractants because it is not metabolized by *B. subtilis* and is toxic. We propose that *B. subtilis* uses ethanol and other short-chain alcohols to locate prey, namely, alcohol-producing microorganisms.

IMPORTANCE Ethanol is a chemoattractant for *Bacillus subtilis* even though it is not metabolized and inhibits growth. *B. subtilis* likely uses ethanol to find ethanol-fermenting microorganisms to utilize as prey. Two chemoreceptors sense ethanol: HemAT and McpB. HemAT's myoglobin-like sensing domain directly binds ethanol, but the heme group is not involved. McpB is a transmembrane receptor consisting of an extracellular sensing domain and a cytoplasmic signaling domain. While most attractants bind the extracellular sensing domain, we found that ethanol directly binds between intermonomer helices of the cytoplasmic signaling domain of McpB, using a mechanism akin to those identified in many mammalian ethanol-binding proteins. Our results indicate that the sensory repertoire of chemoreceptors extends beyond the sensing domain and can directly involve the signaling domain.

KEYWORDS chemotaxis, *Bacillus subtilis*, ethanol sensing, cytoplasmic sensing, chemoreceptor, molecular dynamics, NMR, signal transduction

Many bacteria move in response to external chemical gradients through a process known as chemotaxis (1). Typically, bacteria migrate up gradients of chemicals that support their growth and down ones that inhibit it. These chemicals are commonly

Citation Tohidifar P, Bodhankar GA, Pei S, Cassidy CK, Walukiewicz HE, Ordal GW, Stansfeld PJ, Rao CV. 2020. The unconventional cytoplasmic sensing mechanism for ethanol chemotaxis in *Bacillus subtilis*. mBio 11:e02177-20. <https://doi.org/10.1128/mBio.02177-20>.

Editor Igor B. Zhulin, The Ohio State University

Copyright © 2020 Tohidifar et al. This is an open-access article distributed under the terms of the [Creative Commons Attribution 4.0 International license](https://creativecommons.org/licenses/by/4.0/).

Address correspondence to Christopher V. Rao, cvrao@illinois.edu.

Received 2 August 2020

Accepted 8 September 2020

Published 6 October 2020

sensed using transmembrane chemoreceptors, which consist of an extracellular sensing domain and a cytoplasmic signaling domain along with a cytoplasmic HAMP domain that couples the other two domains. While a number of sensing mechanisms exist, the best-understood one involves the direct binding of the chemical to the extracellular sensing domain (2). In flagellated bacteria such as *Bacillus subtilis* and *Escherichia coli*, this binding event induces a conformational change in the cytoplasmic signaling domain that alters the autophosphorylation rate of an associated histidine kinase known as CheA (3). The phosphoryl group is then transferred to a soluble response regulator known as CheY, which modulates the swimming behavior of the bacterium by changing the direction of flagellar rotation. The chemical gradients themselves are sensed using a temporal mechanism involving sensory adaptation (4).

While many chemicals are sensed by the extracellular sensing domain, some are sensed by the cytoplasmic domains, typically using an indirect mechanism. For example, sugars transported by the phosphoenolpyruvate transfer system (PTS) are indirectly sensed through interactions between the PTS proteins and chemoreceptor signaling complexes (5, 6). In the case of *E. coli*, changes in intracellular pH are sensed by the cytoplasmic HAMP domain (7). The signaling domain of *E. coli* Tar is responsible for the attractant response to toluene and *o*-xylene (8). In addition, changes in osmolarity are sensed through alterations in the packing of the chemoreceptor cytoplasmic signaling domains (9). To our knowledge, however, there have been no reports of direct sensing by the chemoreceptor cytoplasmic signaling domain. This has not been particularly surprising given that the cytoplasmic signaling domain, which consists of a long dimeric four-helix coiled coil (10), lacks an obvious ligand-binding pocket.

In this work, we investigated chemotaxis to ethanol in *B. subtilis*. This short-chain alcohol is an attractant for *B. subtilis* even though it is not used as a carbon source and inhibits cell growth. Ethanol is directly sensed by two chemoreceptors, HemAT and McpB, inside the cytoplasm, where intracellular ethanol concentrations are similar to the extracellular concentrations due to the high permeability of the plasma membrane for short-chain aliphatic alcohols (11–16). Sensing by HemAT fits the conventional model where ethanol binds the cytoplasmic sensing domain. However, in the case of McpB, we found that ethanol is directly sensed by the cytoplasmic signaling domain using a mechanism analogous to those of many eukaryotic ethanol-binding proteins.

RESULTS

***B. subtilis* exhibits chemotaxis to short-chain alcohols.** We employed the capillary assay to measure *B. subtilis* chemotaxis to alcohols with increasing chain lengths (C_1 to C_5). The resulting data show that *B. subtilis* exhibits chemotaxis to methanol, ethanol, 2-propanol, and *tert*-butanol. No significant responses to 1-propanol, 1-butanol, and 1-pentanol were observed (Fig. 1A). To elucidate the underlying sensing mechanism, we focused on ethanol because it is produced and utilized by a wide range of microorganisms in nature (17). We first measured the response to increasing ethanol concentrations using the capillary assay (Fig. 1B). Unlike many other attractants such as amino acids (18–20), a tactic response to ethanol was observed only at relatively high concentrations (>50 mM). The ethanol response peaked at 1.78 M (~10% [vol/vol]). The response decreased at higher concentrations, most likely due to ethanol being toxic at these concentrations (21). It is important to note that the reported alcohol concentrations here are the initial alcohol levels inside the capillaries, and the concentrations sensed by the cells are much lower (see Discussion).

All three adaptation systems contribute to ethanol taxis. *B. subtilis* employs three adaptation systems, the methylation, CheC/CheD/CheYp, and CheV systems, for sensing chemical gradients (4, 22). To test whether these adaptation systems are involved in ethanol taxis, we employed mutants in which these systems were selectively inactivated. We first tested ethanol taxis using a mutant ($\Delta cheC \Delta cheV$) in which the CheC/CheD/CheYp and CheV adaptation systems were inactivated, leaving only the methylation system functional. Taxis to both ethanol and asparagine, which was used as a control, was reduced 30% in this mutant (Fig. 1C). We also observed reduced taxis

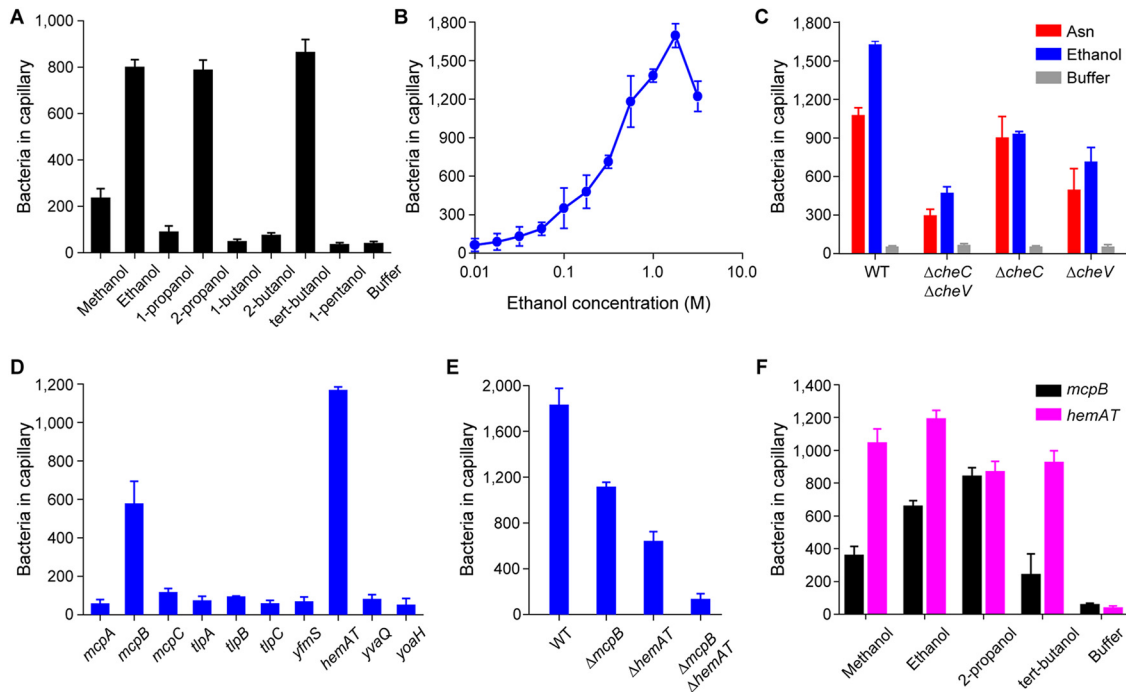


FIG 1 *B. subtilis* exhibits chemotaxis toward short-chain alcohols. (A) Responses of the wild-type strain to 0.5 M short-chain alcohols (in the capillaries) with increasing chain lengths (C_1 to C_5). (B) Dose-dependent responses of the wild-type (WT) strain to increasing concentrations of ethanol. (C) Responses of adaptation-deficient mutants to ethanol and asparagine. (D) Responses of mutants expressing single chemoreceptors to ethanol. (E) Responses of mutants lacking key chemoreceptors to ethanol. (F) Responses of mutants expressing McpB or HemAT as their sole chemoreceptor to short-chain alcohols. In these experiments, ethanol and asparagine concentrations within the capillaries were 1.78 M and 3.16 μ M, respectively, unless otherwise mentioned. The negative-control responses of the strains expressing a single chemoreceptor to buffer were all <100 colonies per capillary. Error bars denote the standard deviations from three biological replicates performed on three separate days.

in the $\Delta cheC$ and $\Delta cheV$ mutants, although the reduction was less than what was observed with the double mutant. Interestingly, the CheC/CheD/CheYp system appears to be more important for sensing ethanol gradients than for sensing asparagine gradients (Fig. 1C). We did not test a $\Delta cheR \Delta cheB$ mutant, which lacks the two enzymes involved in the methylation system, because these mutants exhibit poor motility in general due to excessive tumbling.

McpB and HemAT are the chemoreceptors for short-chain alcohols. *B. subtilis* has 10 chemoreceptors (23). To determine the chemoreceptors involved in ethanol taxis, we first used the capillary assay to test mutants expressing just one chemoreceptor (19, 24, 25). Only strains expressing McpB or HemAT as their sole chemoreceptor were capable of ethanol taxis (Fig. 1D). The response was greater for strains expressing HemAT, suggesting that it is the main receptor for ethanol taxis. This is not surprising, as HemAT is more highly expressed than McpB (19,000 copies versus 6,200 copies) (23). We next tested the effect of deleting these chemoreceptors in the wild type. When either McpB or HemAT was deleted ($\Delta mcpB$ or $\Delta hemAT$), we observed reduced taxis toward ethanol. The reduction was greater in the $\Delta hemAT$ mutant, again suggesting that HemAT is the main receptor for ethanol taxis. When both chemoreceptors were deleted in the wild type ($\Delta mcpB \Delta hemAT$), ethanol taxis was almost eliminated, whereas the mutant exhibited a normal response to proline, an amino acid attractant sensed by McpC ($1,138.7 \pm 34.6$ cells versus $1,276.9 \pm 54.1$ cells for the wild type) (Fig. 1E). We also found that strains expressing McpB or HemAT as their sole chemoreceptor responded to methanol, 2-propanol, and *tert*-butanol (Fig. 1F). Strains expressing HemAT as their sole chemoreceptor exhibited stronger responses to these alcohols than strains expressing McpB alone, with the exception of 2-propanol, where the responses were similar.

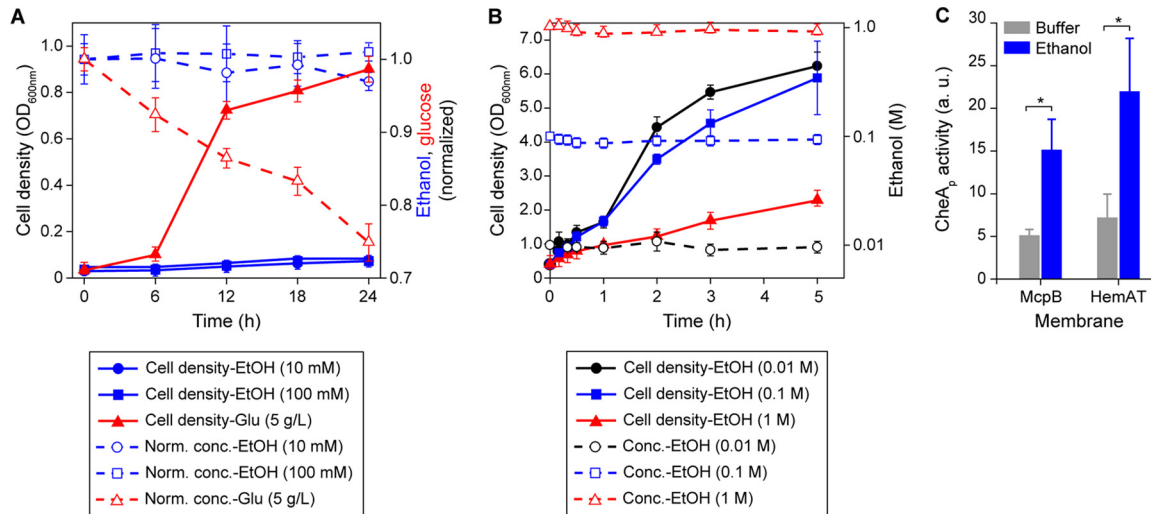


FIG 2 *B. subtilis* chemotaxis to ethanol is independent of its metabolism. (A) Cell growth in minimal medium supplemented with 10 mM ethanol (EtOH), 100 mM ethanol, and 5 g/liter glucose tested as a positive control. Dashed lines with the corresponding symbols depict normalized concentrations of the chemicals measured over the course of 24 h. (B) Cell growth in rich medium containing 10 mM ethanol, 100 mM ethanol, and 1 M ethanol. Dashed lines with open symbols depict absolute concentrations of ethanol measured under three different conditions over the course of 5 h. (C) Levels of phosphorylated CheA kinase complexed with CheW, CheD, and McpB or HemAT within the isolated membranes, in the presence of 1 M ethanol or buffer, as a negative control. Error bars denote the standard deviations from three biological replicates performed on three separate days. a.u., arbitrary units. *, $P < 0.05$ (two-sided t test [correction for unequal variances was applied]).

Chemotaxis to ethanol is independent of its metabolism. Many bacteria metabolize ethanol (26). One possibility is that *B. subtilis* senses products of ethanol metabolism rather than ethanol itself. Indeed, such a mechanism occurs in *Pseudomonas putida* with regard to alcohol taxis (27). Therefore, we tested whether *B. subtilis* can grow on ethanol (Fig. 2A). These growth experiments were performed using the parental strain *B. subtilis* 168, which lacks the auxotrophies present in the chemotaxis strain OI1085. When cells were cultured in minimal medium with ethanol as the sole carbon source, no growth was observed. However, the cells grew when ethanol was replaced with glucose. We also tested *B. subtilis* 168 growth in rich medium containing different amounts of ethanol to determine whether the cells were able to consume ethanol even though it does not support growth as the sole carbon source. While the cells were able to grow in rich medium containing ethanol, no decreases in ethanol concentrations were observed (Fig. 2B). These results indicate that *B. subtilis* does not consume ethanol.

The oxidation of alcohols to aldehydes and subsequently to carboxylic acids can potentially change the redox state of the cells. This change could be perceived as a sensory signal through a process known as energy taxis (28). *B. subtilis* can ferment glucose to acetate and ethanol when grown in the presence of pyruvate or a mixture of amino acids (29, 30). In this process, alcohol dehydrogenase (ADH) reduces acetaldehyde to ethanol using NADH as the cofactor. Whether ADH can oxidize ethanol to acetaldehyde in *B. subtilis* is unknown. To test whether this occurs, we measured ADH activities using *B. subtilis* cell lysates prepared from aerobic and anaerobic cultures. As a positive control, ADH activities using *E. coli* cell lysates were also measured (31). No ADH activity was observed with *B. subtilis* lysates, whereas *E. coli* lysates obtained from anaerobic cultures had an ADH activity of 31.25 ± 1.85 U/ml. As expected, no ADH activity was detected with aerobic *E. coli* lysates. These results suggest that ethanol taxis in *B. subtilis* is independent of ethanol catabolism and is instead sensed directly by McpB and HemAT.

Ethanol induces receptor-coupled kinase activity. We next performed an *in vitro* receptor-coupled kinase assay to test whether ethanol is able to activate CheA kinase (32). This assay has been used to study how attractant binding to chemoreceptors

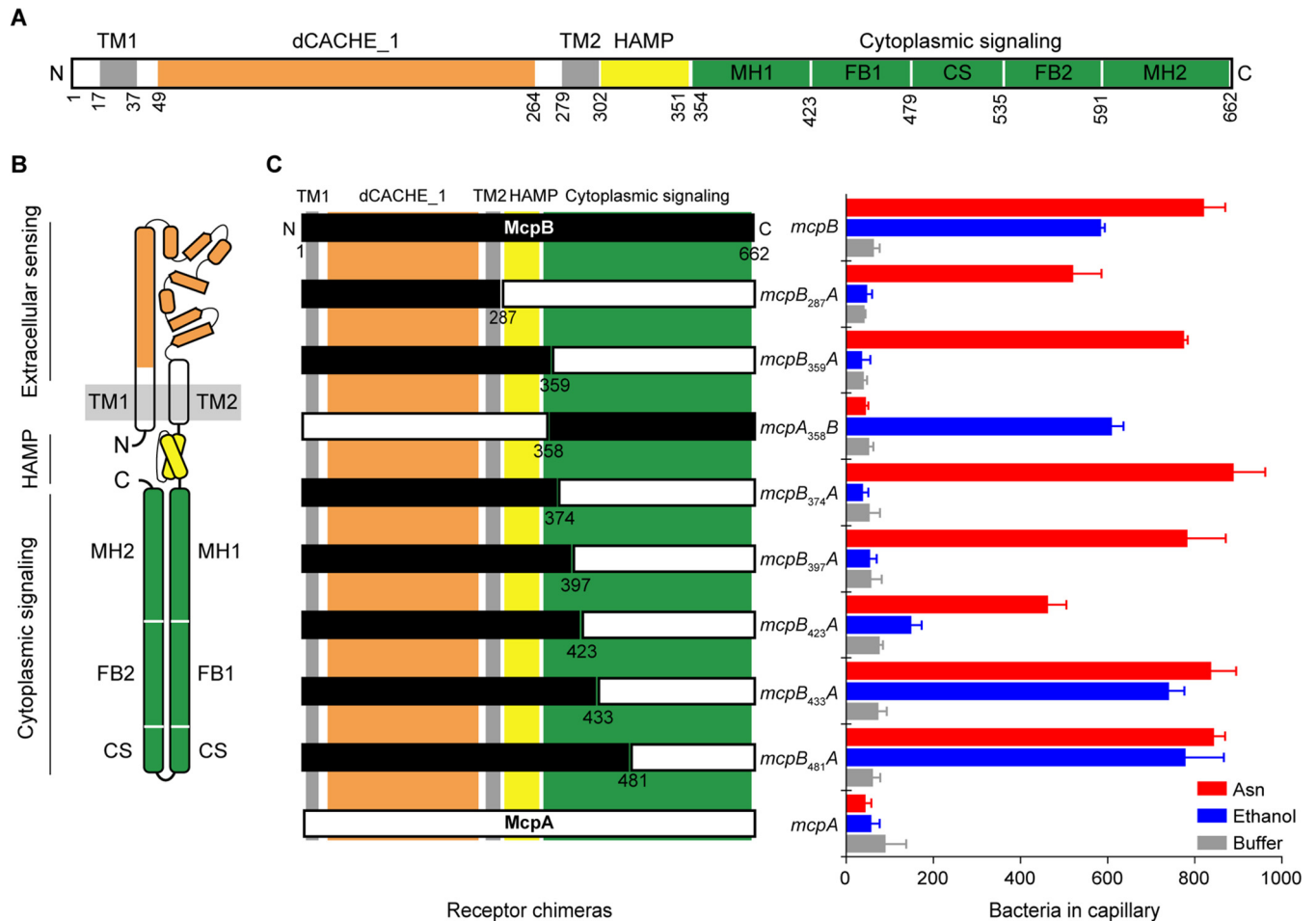


FIG 3 The McpB cytoplasmic signaling domain is involved in ethanol sensing. (A) Domain structures of McpB, McpA, TlpA, and TlpB. All four chemoreceptors consist of an extracellular sensing domain with a dCACHE_1 structure (orange) followed by transmembrane (TM1 and TM2) (gray), HAMP (yellow), and cytoplasmic signaling (green) domains. Three subdomains of the cytoplasmic signaling domain, classified as methylation (adaptation) helices (MH), the flexible (coupling) bundle (FB), and the conserved signaling (CS) (protein contact region) tip, are shown. (B) Cartoon structure of a monomer of the chemoreceptors. (C) Responses of mutants expressing chimeric receptors between McpA (white) and McpB (black) to 1.78 M ethanol, 3.16 μ M asparagine, and buffer. Error bars denote the standard deviations from three biological replicates performed on three separate days.

modulates CheA kinase activity (22, 32). Briefly, membranes expressing either McpB or HemAT were isolated. The chemotaxis signaling proteins CheA, CheW, and CheD were then added to these membranes to final concentrations that matched their stoichiometry in wild-type cells. Using this assay, we found that ethanol activates CheA kinase in a dose-dependent manner with membranes containing either McpB or HemAT as the sole chemoreceptor. Ethanol concentrations as low as 10 mM were sufficient to activate CheA kinase in both cases (Fig. 2C; see also Fig. S1 in the supplemental material). These results indicate that ethanol can induce chemotaxis signaling *in vitro*. This assay, however, is unable to determine whether ethanol directly interacts with the chemoreceptors because the membranes might contain associated proteins that could be involved in signaling.

The McpB cytoplasmic signaling domain is involved in ethanol sensing. We next investigated ethanol taxis using receptor chimeras involving McpB to provide further insight regarding the sensing mechanism (25, 33, 34). We focused on McpB due to its high amino acid similarity (57% to 65%) with three other *B. subtilis* chemoreceptors: McpA, TlpA, and TlpB. These four chemoreceptors all employ the same double Cache 1 sensing domain (2) and a highly conserved coiled-coil structure for their cytoplasmic signaling domain (10) (Fig. 3A and B). Unlike McpB, HemAT is not a transmembrane chemoreceptor. We attempted to construct chi-

meras involving HemAT, McpA, and YfmS, another soluble chemoreceptor. However, none were functional in the sense that they did not respond to ethanol or molecular oxygen, which is the conventional attractant for HemAT (24).

We created chimeras between McpB and McpA because the latter is not involved in ethanol taxis. In addition, we measured the response to asparagine because it is a known attractant for McpB, but not McpA, and it binds the extracellular sensing domain (18). We first fused the N-terminal region of McpB to the C-terminal region of McpA: *mcpB*₂₈₇*A* and *mcpB*₃₅₉*A*. We then tested whether strains expressing these chimeras as their sole chemoreceptor respond to ethanol using the capillary assay. Both mutants failed to respond to ethanol even though they still responded to asparagine (Fig. 3C). These results demonstrate that the extracellular sensing and cytoplasmic HAMP domains are not involved in sensing ethanol. Rather, the cytoplasmic signaling domain is involved. To verify our hypothesis, we tested an *mcpA*₃₅₈*B* chimera. As expected, a strain expressing *mcpA*₃₅₈*B* as its sole chemoreceptor responded to ethanol. This strain, however, does not respond to asparagine because it lacks the requisite McpB sensing domain (Fig. 3C).

Key features of chemoreceptor cytoplasmic signaling domains are the characteristic heptad repeats (labeled *a* to *g*) associated with their coiled-coil structure, where each repeat is equivalent to two helical turns. Based on sequence conservation and structural analyses of heptads from several bacterial and archaeal chemoreceptors, the cytoplasmic signaling domains are classified into three structurally distinct subdomains. These subdomains are known as the methylation (adaptation) helices, the flexible (coupling) bundle, and the conserved signaling tip (protein contact region) (10) (Fig. 3 and Fig. S2). To narrow down the region of these subdomains involved in ethanol sensing, we created *mcpB*₃₇₄*A*, *mcpB*₃₉₇*A*, *mcpB*₄₂₃*A*, *mcpB*₄₃₃*A*, and *mcpB*₄₈₁*A* chimeras. Strains expressing *mcpB*₃₇₄*A* and *mcpB*₃₉₇*A* as their sole chemoreceptor did not respond to ethanol even though they still responded to asparagine. Strains expressing *mcpB*₄₂₃*A* as their sole chemoreceptor exhibited a reduced response to ethanol and asparagine. However, when *mcpB*₄₃₃*A* and *mcpB*₄₈₁*A* were tested, the strains expressing these chimeras were able to respond to ethanol and asparagine at levels similar to those of the wild-type control (Fig. 3C). These results suggest that the region spanning residues 397 to 433 on McpB is involved in sensing ethanol. Furthermore, the region spanning residues 423 to 433 on McpB appears to be the principal region involved in ethanol sensing.

An McpB residue involved in ethanol sensing. The region spanning residues 397 to 433 on McpB is necessary for ethanol taxis. As a first step toward identifying the binding site, we performed *in silico* docking experiments with ethanol and the McpB dimer fragment spanning residues 390 to 435 on the N-helix and the neighboring residues 577 to 622 on the C-helix. The resulting data from the docking analysis yielded five distinct clusters of putative amino acid residues involving both the N-helix and the C-helix of the dimer fragment (Table S1 and Fig. S3A). We next aligned the amino acid sequences spanning residues 392 to 434 on the N-helix and the neighboring residues 578 to 620 on the C-helix of McpB, McpA, TlpA, and TlpB (Fig. S3B). Among the 20 putative binding residues, Thr⁴²⁴, Asp⁴²⁷, and Ala⁴³¹ on the N-helix and Glu⁵⁸¹ and Lys⁵⁸⁵ on the C-helix were not conserved between the four chemoreceptors and, thus, were targeted for mutational analysis (Fig. 4A and B). Mutants expressing McpB-T424A, McpB-D427T, McpB-E581Q, and McpB-K585E as their sole chemoreceptor exhibited responses to ethanol similar to those of wild-type *mcpB*. However, the strain expressing McpB-A431S as its sole chemoreceptor failed to respond to ethanol. In addition, all strains supported asparagine taxis, indicating that these mutated receptors were functional (Fig. 4C). We also measured the responses of the strain expressing McpB-A431S to methanol, 2-propanol, and *tert*-butanol in the capillary assay and observed reduced responses (Fig. 4D), suggesting that Ala⁴³¹ is an important residue for alcohol taxis overall.

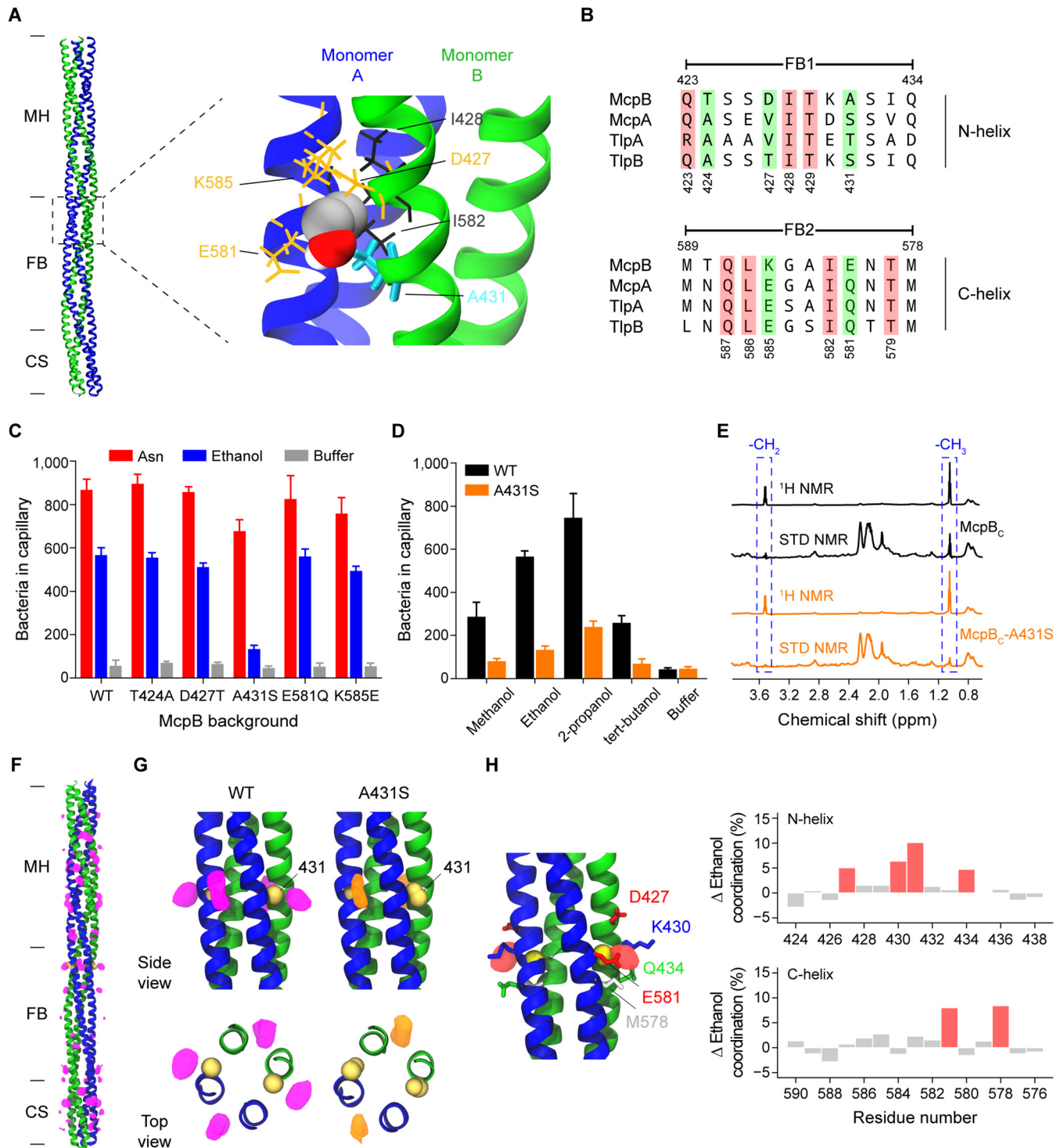


FIG 4 Alcohols are directly sensed by the cytoplasmic signaling domain of McpB. (A) Putative binding site within the primary ethanol-sensing region spanning residues 423 to 433 on the N-helix and the neighboring residues 579 to 589 on the C-helix of the McpB cytoplasmic signaling domain. (B) Amino acid sequence alignment of the primary ethanol-sensing region for McpB and the corresponding regions on McpA, TlpA, and TlpB. (C) Responses of strains expressing McpB mutants as their sole chemoreceptor to 1.78 M ethanol, 3.16 μ M asparagine, and buffer. (D) Responses of strains expressing wild-type McpB and the McpB-A431S mutant as their sole chemoreceptor to 1.78 M short-chain alcohols and buffer. (E) ^1H and STD-NMR spectra for 50 μ M wild-type and mutant (A431S) recombinant McpB cytoplasmic regions (McpB_c) spanning residues 305 to 662. Two peaks at 1.05 ppm and 3.51 ppm (shown inside dashed boxes) correspond to $-\text{CH}_3$ and $-\text{CH}_2$ epitopes of ethanol, respectively. (F) Density map of the average ethanol occupancy (purple) along the wild-type McpB cytoplasmic signaling domain (McpB_c) spanning residues 352 to 662, as predicted by MD simulation. (G) Enlarged side and top views of the ethanol occupancy surrounding residue 431 (yellow) in wild-type (purple) and A431S mutant (orange) McpB_c. (H) Difference map (red density) between wild-type and A431S mutant McpB_c surrounding residue 431 highlighting the loss of an intermonomer ethanol-binding site in the A431S mutant. Changes in protein-ethanol coordination highlight the putative amino acid residues (red bars) involved in ethanol binding. Error bars reported in panels C and D denote the standard deviations from three biological replicates performed on three separate days. Ethanol occupancy and coordination values were generated from three independent MD simulations.

Ethanol directly binds to the McpB cytoplasmic signaling domain. To test whether ethanol directly interacts with McpB, we conducted saturation transfer difference nuclear magnetic resonance (STD-NMR) experiments using recombinant McpB. STD-NMR has been used to measure weak interactions between proteins and their ligands (35–38). Briefly, in these experiments, the protein is selectively saturated at specific frequencies. The magnetization is then transferred to the surrounding, low-molecular-weight ligands in a distance-dependent manner. The ligand epitopes near the protein receive higher saturation (39), implying direct binding to the protein.

We first tested the McpB cytoplasmic region (McpB_C) spanning residues 305 to 662, which corresponds to the HAMP and signaling domains (Fig. 3A). The resulting ¹H spectrum for the McpB_C protein incubated with 3 mM ethanol (60-fold molar excess of the protein) is shown in Fig. 4E. Two peaks for ethanol appeared near 1.05 ppm and 3.51 ppm, which correspond to the -CH₃ and -CH₂ epitopes of ethanol, respectively. Ligand signals were also observed at the expected chemical shift values (1.05 ppm and 3.51 ppm) on the STD spectra. Additionally, the area under the STD peak corresponding to the -CH₂ epitope was about 5-fold (18%) smaller than that of the -CH₃ epitope (Fig. 4E), suggesting that the -CH₃ moiety of ethanol is closer to the protein than its -CH₂ moiety. Moreover, control experiments using 3 mM 1-pentanol, which is not an attractant, and McpB_C showed negligible STD peaks near the characteristic chemical shift values (3.5, 1.41, 1.18, and 0.8 ppm), suggesting that 1-pentanol does not bind McpB_C (Fig. S4A). As an additional negative control, we performed STD-NMR experiments using the McpA cytoplasmic region spanning residues 305 to 661 with 3 mM ethanol. Consistent with our *in vivo* results, we did not observe significant STD peaks near the characteristic chemical shift values (Fig. S4A). These results collectively indicate that ethanol directly interacts with the McpB cytoplasmic region.

Strains expressing McpB-A431S as their sole chemoreceptor exhibited a reduced response to ethanol when tested in the capillary assay (Fig. 4C). To determine whether the A431S mutation reduces ethanol binding, we repeated the STD-NMR experiments with the recombinant McpB_C-A431S protein. Because single mutations may impair the proper folding of proteins, we first measured the circular dichroism (CD) spectra for both the wild-type McpB_C and the McpB_C-A431S proteins. We observed similar spectra for both proteins, which suggests that the mutant protein preserves the wild-type helical structure (Fig. S4B). We then performed STD-NMR experiments with McpB_C-A431S in the presence of 3 mM ethanol. The resulting STD spectra showed reduced peaks near 1.05 ppm and 3.51 ppm compared to wild-type McpB_C (Fig. 4E). The saturation fractions of ethanol, which correspond to the ratios of the areas under the respective -CH₃ peaks on STD and ¹H spectra, are 0.23 for McpB_C and 0.1 for McpB_C-A431S. These results imply that residue Ala⁴³¹ has a role in ethanol binding to the McpB signaling domain.

Molecular dynamics simulation suggests the A431S mutation reduces the affinity of ethanol for the McpB cytoplasmic signaling domain. To gain insight regarding the ethanol-binding mechanism, we performed molecular dynamics (MD) simulations of the wild-type and A431S McpB cytoplasmic signaling dimers (residues 352 to 662) in the presence of ethanol. Our simulations demonstrate that ethanol can bind nonspecifically throughout the cytoplasmic signaling domain in both the wild-type and mutant McpB dimers, primarily interacting along the interhelical grooves of the four-helix bundle (Fig. 4F and Fig. S5A). A comparison of ethanol occupancies between wild-type and A431S mutant McpB showed little variation overall but exhibited a marked difference in the region immediately surrounding residue 431. In particular, while ethanol was observed to bind at both the inter- and intramonomer interfaces in the wild-type simulations, the intermonomer binding site associated with the residue 431 side chain was not present in the mutant simulations (Fig. 4G), suggesting that the A431S mutation reduces the binding affinity of ethanol. Indeed, within the flexible-bundle region, the residues displaying the greatest change in

ethanol coordination between the wild type and the A431S mutant form a concentric pocket centered on residue 431 at the intermonomer interface (Fig. 4H).

Our analyses identified another interesting feature of ethanol binding, namely, that it is able to penetrate the surface of the McpB cytoplasmic domain to bind within the core of the coiled coil. In particular, we observed that ethanol entered between the individual helices of the four-helix bundle at two locations in the methylation-helix region: one involving N-helix residues 393 to 400 and C-helix residues 613 to 617 and the other involving N-helix residues 382 to 387 and C-helix residues 628 to 631 (Fig. S5A). While ethanol binding to these regions was observed in both the wild-type and A431S mutant simulations, the wild-type binding events resulted in longer dwell times, giving rise to the difference in ethanol coordination observed in these regions (Fig. S5A). Preliminary analysis of the two sites, however, suggests that they do not themselves play a significant role in signaling. The latter is located outside the region involved in ethanol sensing (Fig. 3C), and the former, except for residue Glu³⁹⁹, is highly conserved among the four chemoreceptors (Fig. S3B). Indeed, we did not observe a significant reduction in response to ethanol compared to the wild-type control when we tested a mutant expressing McpB-E399K as its sole chemoreceptor in the capillary assay (569 ± 29.1 cells versus 586.1 ± 9.0 cells, respectively). Nevertheless, these observations hint at a signaling mechanism in which ethanol may penetrate to the core of the cytoplasmic domain, where it can affect the packing and overall stability of the bundle.

To investigate the above-described packing hypothesis further, we analyzed the strength of knobs-in-holes interactions in the region surrounding residue 431 over the course of the simulations. We observed that the A431S mutation leads to an increased occupancy of the residue 431 knob itself as well as nearby knobs on the C-helix at positions 583 and 585 (Fig. S5B), indicating stronger hydrophobic interactions between the individual helices. Therefore, our simulation results suggest that the A431S substitution, which decreases the McpB ethanol response, not only reduces the direct binding of ethanol but also strengthens coiled-coil packing in the region. One possibility is that the reduced local concentration of ethanol and improved packing in the A431S mutant decrease the ability of ethanol to intercalate with the knobs-into-holes interactions near residue 431 and, thus, its ability to induce signaling.

The HemAT sensing domain helices are directly involved in ethanol sensing.

HemAT is a cytoplasmic chemoreceptor that consists of an N-terminal sensing domain and a C-terminal signaling domain. To determine whether the HemAT signaling domain is also involved in ethanol sensing, we conducted STD-NMR experiments with the purified signaling domain (HemAT_S), spanning residues 177 to 432, and the purified sensing domain (HemAT_N), spanning residues 1 to 178, of HemAT in the presence of 3 mM ethanol. The STD spectra with the HemAT signaling domain showed negligible peaks near the expected chemical shift values (1.05 ppm and 3.51 ppm), while the resulting ¹H and STD spectra with HemAT_N showed clear peaks near 1.05 ppm and 3.51 ppm, which correspond to the -CH₃ and the -CH₂ moieties of ethanol. The ratios of the areas in the STD spectra to those in the ¹H spectra were 0.27 for the -CH₃ moiety and 0.85 for the -CH₂ moiety, suggesting that the -CH₂ moiety of ethanol is closer to the protein than its -CH₃ moiety (Fig. 5A). These results collectively indicate that ethanol binds the sensing domain of HemAT.

The sensing domain of the HemAT dimer is composed of a four-helical bundle as its core and a heme group in each subunit (Fig. 5B), which is known to bind molecular oxygen (40). UV spectral analyses have shown that the oxygen molecule binds the heme group by forming hydrogen bonds with 6-coordinate ferrous heme (41, 42). To determine whether the heme group also interacts with ethanol, we conducted UV spectroscopy experiments with the purified HemAT sensing domain (HemAT_N) and ethanol. As a control, we first measured the UV absorption of both oxygenated and deoxygenated forms of the protein to verify that the heme group on the purified protein is functional. Consistent with previous reports (24, 41, 43), the oxygenated form of HemAT_N exhibited three major canonical peaks at 412 nm (Soret), 544 nm (β-band),

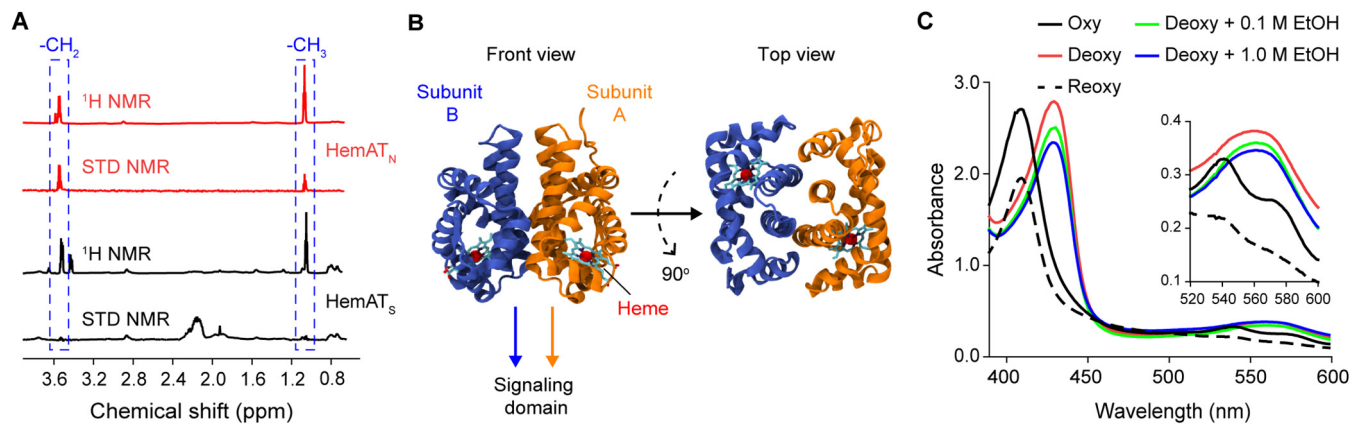


FIG 5 Ethanol directly binds within the helices of the HemAT sensing domain. (A) ¹H and STD-NMR spectra for 50 μM the recombinant HemAT C-terminal signaling domain (HemAT_S) spanning residues 177 to 432 and for 50 μM the recombinant HemAT N-terminal sensing domain (HemAT_N) spanning residues 1 to 178, in the presence of 3 mM ethanol. Two peaks at 1.05 ppm and 3.51 ppm (shown inside dashed boxes) correspond to -CH₃ and -CH₂ epitopes of ethanol, respectively. (B) Crystal structure of the dimeric HemAT sensing domain. (C) UV spectra of recombinant HemAT_N in the absence and presence of molecular oxygen, 0.1 M ethanol, and 1.0 M ethanol.

and 578 nm (α -band), and the dithionite-reduced deoxygenated form of the protein exhibited two major peaks at 434 nm and 556 nm (Fig. 5C). Next, we measured the UV absorption of the deoxygenated HemAT sensing domain in the presence of various concentrations of ethanol. The resulting spectra showed two major peaks at 434 nm and 556 nm, similar to what we observed with the deoxygenated form of the protein in the absence of any ligand (Fig. 5C). These results imply that the heme group does not interact with ethanol. Rather, they suggest that ethanol binds to the alpha helices of the HemAT sensing domain. It is noteworthy that while ethanol binds to the alpha helices in both McpB and HemAT, the binding mode appears to be different. The STD-NMR experiments suggest that the -CH₃ moiety of ethanol is closer to McpB than its -CH₂ moiety, whereas the ethanol binding direction is reversed in the case of HemAT.

DISCUSSION

We found that *B. subtilis* performs chemotaxis to multiple short-chain alcohols. These alcohols are directly sensed by two chemoreceptors, McpB and HemAT. McpB is a transmembrane chemoreceptor with an extracellular sensing domain and a cytoplasmic signaling domain, which are linked by a cytoplasmic HAMP domain. It is known to sense the amino acid asparagine and alkaline environments as attractants using the extracellular sensing domain (18, 25). HemAT, on the other hand, is a soluble chemoreceptor that consists of a sensing and a signaling domain but lacks a HAMP domain. Its myoglobin-like sensing domain contains heme and is known to bind molecular oxygen (24, 42). Using chimeric receptors and STD-NMR, we found that short-chain alcohols are directly sensed by the cytoplasmic signaling domain of McpB and the sensing domain of HemAT. In the case of HemAT, the alcohols do not appear to bind heme; rather, they likely bind between the helices encapsulating the heme.

Among the alcohols tested, ethanol is the most likely physiological attractant because it is produced by many microorganisms and is prevalent in nature (17). As a consequence, we focused on this chemical. Curiously, ethanol is not consumed by *B. subtilis*, suggesting that it is used for purposes other than nutrition. One possibility is that *B. subtilis* uses ethanol to locate prey, which could explain why *B. subtilis* is attracted to a chemical that nominally inhibits its growth. The most likely prey are Crabtree-positive yeast such as *Saccharomyces cerevisiae*, which produces ethanol at high concentrations even during aerobic growth (44). Indeed, *B. subtilis* can lyse *S. cerevisiae* cells through the production of cell wall-degrading compounds (see Fig. S6 in the supplemental material) (45–47).

Aside from ethanol, methanol may also be a physiological attractant. It is a by-product of pectin degradation and, as a consequence, can contaminate alcoholic

beverages (48). However, *B. subtilis* does not consume methanol because it lacks methanol dehydrogenase activity (49). Similar to ethanol, *B. subtilis* may use methanol to locate prey, in this case pectin-degrading microorganisms.

These speculations are in line with the results from a previous study where no correlation was observed between the metabolic and chemotactic preferences of *B. subtilis* for amino acids (50). That study proposed that *B. subtilis* uses amino acid gradients as cues to locate sources of nutrients, for example, during plant root colonization (50, 51). The only other bacterium known to exhibit taxis toward alcohols is *Pseudomonas putida* (27). However, this bacterium consumes alcohols. In addition, it does not directly sense these alcohols but rather senses the by-products of their degradation, namely, carboxylic acid. Finally, alcohol taxis is also observed in *E. coli* and *Ralstonia pseudosolanacearum*. In these bacteria, however, alcohols are sensed as repellents (52, 53).

A key difference between taxis to alcohols and conventional attractants such as amino acids is their respective sensitivities. Amino acids are sensed at micromolar concentrations, whereas alcohols are sensed at millimolar concentrations. However, it should be noted that while low millimolar concentrations (e.g., 3 mM) of ethanol can bind McpB and HemAT *in vitro*, much higher ethanol levels are required for optimal chemotaxis in the capillary assay experiments. The disparity may be due to the architecture of the capillary assay. Briefly, chemotaxis to ethanol occurs when ethanol concentrations in the capillaries are as low as 50 mM (190.1 ± 44.5 cells versus 42.3 ± 6.2 cells for buffer), and the response to ethanol peaks when capillaries contain about 2 M ethanol. These concentrations, however, do not reflect the ethanol concentrations that cells experience near the mouth of the capillary in the pond. Three-dimensional simulations based on finite-element analysis of ethanol diffusion from a capillary into a pond indicate that the ethanol concentration falls dramatically, 10 to 50 times, compared with the initial ethanol concentration in the capillary near the mouth of the capillary (distances of <0.5 mm) (Fig. S7). These simulation results suggest that cells are able to respond to ethanol levels ranging from 1 to 200 mM. That said, the weak affinity for alcohols is not surprising because most ethanol receptors in mammals also exhibit a weak affinity for ethanol (54).

The question, then, is whether ethanol is actually an attractant for *B. subtilis* given that relatively high concentrations are necessary to elicit taxis. Overripe fruits provide one potential source for high ethanol concentrations, where concentrations can exceed 1 M (55). In addition, flooded plant roots can provide another source at millimolar concentrations (56–58). In this case, *B. subtilis* perhaps uses ethanol to locate roots for colonization to initiate symbiosis (51). These observations suggest that ethanol taxis can indeed occur in the environment. Whether the other alcohols reach such concentrations in the environment is not known.

Perhaps the most interesting aspect of ethanol taxis involves the sensing mechanism. Typically, small-molecule attractants bind the extracellular sensing domain. The main exceptions are PTS sugars, which are sensed indirectly through the PTS system (5, 6). Ethanol is sensed intracellularly. In the case of HemAT, this distinction is minor, as ethanol binds the sensing domain albeit one normally associated with oxygen sensing. In the case of McpB, the cytoplasmic signaling domain is involved in sensing ethanol through direct binding. This appears to be the first documented case of the cytoplasmic signaling domain being directly involved in sensing. While we were able to establish that ethanol binds the McpB cytoplasmic signaling domain using genetics and STD-NMR, the details of the binding and signaling mechanisms are still somewhat opaque. In particular, it is not clear whether ethanol exerts its effect precisely at residue 431 or possibly at one or multiple other positions along the lengthy cytoplasmic domain. Molecular dynamics simulations suggest that ethanol can bind nonspecifically at several places on the McpB cytoplasmic surface as well as penetrate to the core of the four-helix bundle, at least within the methylation helix region. Although we did not observe ethanol entering the bundle core near residue 431 in our simulations, it may do so on longer time scales or in particular signaling states. In addition, precise

molecular details of how ethanol binding induces signaling in wild-type McpB remain to be worked out. The enhanced packing interactions in McpB-A431S, which does not respond to ethanol, suggest that A431 may disrupt or loosen packing, leading to changes in the overall stability of McpB that can be transmitted to the kinase. This idea is in line with numerous previous studies of the *E. coli* Tsr and Tar chemoreceptors, for example, that suggest that changes in periplasmic ligand binding and the adaptation state affect packing throughout the cytoplasmic bundle (5, 6).

Many aspects of ethanol sensing in *B. subtilis* are analogous to mechanisms observed in higher eukaryotes. Alcohols generally bind to proteins with low affinities, and relatively high concentrations of alcohols are required to induce behavioral effects. For example, ligand-gated ion channel receptors such as the *N*-methyl-D-aspartate (NMDA)-type glutamate receptors, γ -aminobutyric acid type A (GABA_A) receptors, and glycine receptors all exhibit weak affinities for ethanol (>10 mM) (54). Although the binding sites on these proteins are not well characterized, ethanol is thought to bind helical regions in most cases. In the case of the GABA_A receptor, for example, ethanol binds within a small cavity between two transmembrane helices (TM2 and TM3) (59). Molecular dynamics studies show that ethanol modulates the receptor states by stabilizing helical crossing angles with a “wringing motion” (60, 61). Ethanol inhibition of the NMDA receptor is regulated by counteracting forces on M3 helices of the receptors with additional interactions with side chains (62). Potassium channels are also affected by >100 mM ethanol concentrations. Kinetic and structural studies of Shaw2 K⁺ channels have shown that the alpha-helical propensity of the loop in the pore-forming subunit is important for ethanol binding (63). Similarly, in the case of the odorant-binding protein LUSH from *Drosophila melanogaster*, a small cavity between the alpha helices accommodates a single ethanol molecule, whose hydroxyl group forms hydrogen bonds with neighboring threonine (Thr⁵⁷) and serine (Ser⁵²) residues (64). The binding motif found in LUSH is shared by the GABA_A receptor, the glycine receptor, and the *Drosophila* Shaw2 K⁺ channel (64), suggesting a common alcohol-binding mechanism in eukaryotes.

Experimental and computational studies of the ion channel GLIC in the bacterium *Gloeobacter violaceus* also point to a mechanism of alcohol binding within cavities between transmembrane helices (65). Analysis of binding sites from structural studies suggests that ethanol preferentially binds helices with amphipathic surfaces (54, 66, 67). The sensing mechanisms for these proteins typically involve the replacement of water molecules with ethanol within small hydrophobic cavities between two or more helices. Indeed, an analogous mechanism appears to be employed by the *B. subtilis* chemoreceptors. Given the reported similarities in the modes of action of ethanol in both prokaryotic and eukaryotic proteins, the model hypothesized in this investigation could provide evolutionary clues on the mechanisms of alcohol-sensing proteins.

MATERIALS AND METHODS

Chemicals and growth media. The following media were used for cell growth: Luria-Bertani (LB) broth (1% tryptone, 0.5% yeast extract, and 0.5% NaCl), tryptone broth (TB) (1% tryptone and 0.5% NaCl), tryptone blood agar base (TBAB) (1% tryptone, 0.3% beef extract, 0.5% NaCl, and 1.5% agar), yeast-peptone-dextrose (YPD) broth (1% yeast extract, 2% peptone, and 2% dextrose), and capillary assay minimal medium (CAMM) [50 mM potassium phosphate buffer (pH 7.0), 1.2 mM MgCl₂, 0.14 mM CaCl₂, 1 mM (NH₄)₂SO₄, 0.01 mM MnCl₂, and 42 μM ferric citrate]. Chemotaxis buffer consists of 10 mM potassium phosphate buffer (pH 7.0), 0.14 mM CaCl₂, 0.3 mM (NH₄)₂SO₄, 0.1 mM EDTA, 5 mM sodium lactate, and 0.05% (vol/vol) glycerol. All alcohols used in this study were purchased from Fisher Scientific, Inc.

Strains and plasmids. All strains and plasmids used in this work are listed in Tables 1 and 2, respectively. Chemotaxis experiments were performed with derivatives of *B. subtilis* OI1085. Growth experiments were performed using *B. subtilis* 168, which is the parental strain. The undomesticated *B. subtilis* strain NCBI 3610 and the *Saccharomyces cerevisiae* CEN.PK113-7D yeast strain were used in the antimicrobial diffusion assays. All cloning was performed using NEB 5-alpha competent *E. coli* (New England Biolabs). All oligonucleotides used in this study are provided in Table S2 in the supplemental material.

Gene deletions were constructed using plasmids derived from pJSpe, which provides a CRISPR/Cas9-based, marker-free, and scarless genome-editing system for *B. subtilis* (68). To construct a deletion vector, a 20-bp CRISPR RNA target sequence complementary to the targeted gene sequence was designed using

TABLE 1 Strains used in this study

Strain	Relevant genotype or description	Source or reference
5-alpha	<i>E. coli</i> cloning host	New England BioLabs
BL21(DE3)	<i>E. coli</i> protease-deficient expression host	Novagen
GBS111	<i>Saccharomyces cerevisiae</i> CEN.PK113-7D	
NCBI3610	Undomesticated wild-type <i>B. subtilis</i> isolate	
OI3269	<i>Bacillus subtilis</i> 168 <i>trpC2</i>	
OI1085	<i>trpF7 hisH2 metC133 che⁺</i>	97
PTS375	Δ <i>cheC</i> Δ <i>cheV</i>	This work
PTS097	Δ <i>cheC</i>	25
PTS135	Δ <i>cheV</i>	25
PTS185	Δ <i>mcpB</i>	25
PTS328	Δ <i>hemAT</i>	This work
PTS238	Δ <i>mcpB</i> Δ <i>hemAT</i>	This work
OI3545	Δ 10 <i>mcp</i> <i>Erm^r Cm^r Kan^r che⁺</i>	24
OI3921	OI3545 <i>amyE5720::mcpA</i> <i>Spc^r</i>	98
OI3605	OI3545 <i>amyE5720::mcpB</i> <i>Spc^r</i>	5
OI3974	OI3545 <i>amyE5720::mcpC</i> <i>Spc^r</i>	5
OI4474	OI3545 <i>amyE5720::tlpA</i> <i>Spc^r</i>	25
OI4475	OI3545 <i>amyE5720::tlpB</i> <i>Spc^r</i>	25
OI4483	OI3545 <i>amyE5720::tlpC</i> <i>Spc^r</i>	25
OI4476	OI3545 <i>amyE5720::yfmS</i> <i>Spc^r</i>	25
OI4477	OI3545 <i>amyE5720::yvaQ</i> <i>Spc^r</i>	25
OI4482	OI3545 <i>amyE5720::hemAT</i> <i>Spc^r</i>	25
OI4479	OI3545 <i>amyE5720::yohaH</i> <i>Spc^r</i>	25
PTS522	OI3545 <i>amyE5720::mcpB</i> [M1-V287] <i>mcpA</i> [L287-E661]	This work
PTS529	OI3545 <i>amyE5720::mcpB</i> [M1-Q359] <i>mcpA</i> [D359-E661]	This work
GBS103	OI3545 <i>amyE5720::mcpB</i> [M1-A374] <i>mcpA</i> [S374-E661]	This work
GBS104	OI3545 <i>amyE5720::mcpB</i> [M1-N397] <i>mcpA</i> [E397-E661]	This work
GBS142	OI3545 <i>amyE5720::mcpB</i> [M1-Q423] <i>mcpA</i> [A423-E661]	This work
GBS090	OI3545 <i>amyE5720::mcpB</i> [M1-I433] <i>mcpA</i> [Q433-E661]	This work
GBS091	OI3545 <i>amyE5720::mcpB</i> [M1-I481] <i>mcpA</i> [Q433-E661]	This work
PTS252	OI3545 <i>amyE5720::mcpA</i> [M1-Q358] <i>mcpB</i> [D359-E662]	This work
GBS149	OI3545 <i>amyE5720::mcpB</i> [A431S]	This work
GBS176	OI3545 <i>amyE5720::mcpB</i> [T424A]	This work
GBS175	OI3545 <i>amyE5720::mcpB</i> [D427T]	This work
GBS158	OI3545 <i>amyE5720::mcpB</i> [E581Q]	This work
GBS170	OI3545 <i>amyE5720::mcpB</i> [K585E]	This work
GBS192	OI3545 <i>amyE5720::mcpB</i> [E399K]	This work

the CHOPCHOP online tool (69). The 5'-end-phosphorylated complementary oligonucleotides were then annealed and subcloned into BsaI restriction sites on the pJSpe plasmid using Golden Gate assembly (70). The resultant plasmid was then linearized at the SpeI restriction site and joined to two PCR fragments (~700 to 800 bp) flanking the targeted gene using Gibson assembly (71). Prior to transformation into the *B. subtilis* strain, each of the pJSpe-derived deletion plasmids was linearized at the XhoI restriction site and subsequently self-ligated to create a long DNA concatemer. The concatemer was then transformed into the *B. subtilis* strain using the two-step Spizizen method (72). The transformation product of the *B. subtilis* strain and the deletion plasmid concatemer was incubated on an LB agar (LB medium and 1.5% agar) plate supplemented with 5 μ g/ml kanamycin and 0.2% mannose for about 24 h at 30°C. Next, single colonies were isolated and streaked twice onto fresh drug-containing plates (described above) to ensure a clonal genotype. Positive colonies were verified using colony PCR, again streaked onto a plain LB agar plate, and incubated for an additional 24 h at 50°C to cure the deletion plasmid. Colonies with cured plasmids were unable to grow on an LB agar plate supplemented with 5 μ g/ml kanamycin.

To construct chemoreceptor chimeras, two opposing primers were designed to amplify DNA regions outward from the fusion points of the chimeric gene using PCR with the pAIN750*mcpB* integration plasmid as the DNA template. Next, a second pair of primers with short overlapping regions was used to PCR amplify the desired fragment of the *mcpA* gene from pAIN750*mcpA*. Following the purification of PCR DNA products by gel extraction, the DNA fragments were assembled using Gibson assembly and transformed into *E. coli*. Following isolation from *E. coli* and sequence verification, the concatemer of the resultant integration plasmid was prepared as described above and transformed into *B. subtilis* OI3545, which lacks all 10 chemoreceptors. The transformation product was then incubated on an LB agar plate supplemented with 100 μ g/ml spectinomycin for 15 h at 37°C. Single colonies were isolated and streaked onto a TBAB agar (TBAB and 1.5% agar) plate supplemented with 1% soluble starch. A single positive colony with the chemoreceptor expression cassette recombined to the *amyE* locus was verified using a Gram iodine solution (0.33% iodine, 0.66% potassium iodide, and 1% sodium bicarbonate). Correct colonies with a disrupted *amyE* gene were unable to form clear zones on a TBAB-starch plate.

Point mutations on the *mcpB* chemoreceptor gene were introduced using the inverse PCR method. Briefly, two opposing primers containing the desired mutations were used to PCR amplify the

TABLE 2 Plasmids used in this study

Plasmid	Description	Source or reference
pET28a(+)	His-tagged cloning vector for protein purification; Kan ^r	Novagen
pJSpe	Modified pJOE8999 optimized for Gibson assembly of homology templates; Amp ^r Kan ^r	25
pPT037	pJSpe::cheV (for cheV knockout)	25
pPT058	pJSpe::mcpB (for mcpB knockout)	25
pPT053	pJSpe::hemAT (for hemAT knockout)	This work
pAIN750	<i>B. subtilis</i> empty vector for integration at amyE; Amp ^r Spc ^r	98
pPT200	pAIN750::mcpB[M1-V287] mcpA[L287-E661]	This work
pPT205	pAIN750::mcpB[M1-Q359] mcpA[D359-E661]	This work
pGB42	pAIN750::mcpB[M1-A374] mcpA[S374-E661]	This work
pGB43	pAIN750::mcpB[M1-N397] mcpA[E397-E661]	This work
pGB34	pAIN750::mcpB[M1-I433] mcpA[Q433-E661]	This work
pGB64	pAIN750::mcpB[M1-Q423] mcpA[A423-E661]	This work
pGB35	pAIN750::mcpB[M1-L481] mcpA[R481-E661]	This work
pPT086	pAIN750::mcpA[M1-Q358]-mcpB[D359-E662]	This work
pGB65	pAIN750::mcpB[A431S]	This work
pGB83	pAIN750::mcpB[T424A]	This work
pGB82	pAIN750::mcpB[D427T]	This work
pGB67	pAIN750::mcpB[E581Q]	This work
pGB79	pAIN750::mcpB[K585E]	This work
pGB94	pAIN750::mcpB[E399K]	This work
pPT262	His ₆ -C-terminal McpB expression plasmid, pET28(a)::mcpB _C	This work
pGB78	His ₆ -C-terminal McpB _C -A431S expression plasmid, pET28(a)::mcpB _C [A431S]	This work
pGB53	His ₆ -C-terminal McpA expression plasmid, pET28(a)::mcpA _C	This work
pGEX-6p-2::cheA	GST-CheA overexpression plasmid	22
pGEX-6p-2::cheW	GST-CheW overexpression plasmid	22
pGEX-6p-2::cheD	GST-CheD overexpression plasmid	22
pGB46	His ₆ -C-terminal HemAT expression plasmid, pET28(a)::hemAT ₅	This work
pSP03	His ₆ -N-terminal HemAT expression plasmid, pET28(a)::hemAT _N	This work

pAIN750mcpB integration plasmid. Following the purification of PCR DNA by gel extraction, the 5' end of the DNA fragment was phosphorylated with T4 polynucleotide kinase and then blunt-end ligated using T4 DNA ligase. The ligation product was heat inactivated and transformed into *E. coli*. Following isolation from *E. coli* and sequence verification, the concatemer of the resultant integration plasmid was prepared as described above and transformed into *B. subtilis* OI3545 to integrate the mutant chemoreceptor expression cassette into the amyE locus.

Protein expression plasmids were constructed with the pET28(+) expression vector system using Gibson assembly. Briefly, DNA for the HemAT sensing domain (residues 1 to 178) was cloned in frame with a C-terminal His₆ tag between the NcoI and HindIII restriction sites on pET28a(+). Similarly, the DNAs for the wild-type McpB, wild-type McpA, and McpB-A431S cytoplasmic regions, including the HAMP domain (residues 305 to 662 for McpB and residues 304 to 661 for McpA), were cloned in frame with a C-terminal His₆ tag at the NcoI restriction site on pET28a(+). The DNA for the HemAT signaling domain (residues 177 to 432) was cloned in frame with an N-terminal His₆ tag at the NheI restriction site on pET28a(+). After isolation and sequence verification, all plasmids were transformed into the *E. coli* BL21(DE3) strain for protein expression and purification.

Protein expression and purification. The CheA, CheW, and CheD proteins used in the kinase assay were expressed from glutathione S-transferase (GST) fusion plasmids and purified from the *E. coli* BL21(DE3) strain as described previously (22, 32). GSTrap columns (5 ml; GE Healthcare) were used with an Äkta Prime fast protein liquid chromatography (FPLC) system (GE Healthcare) for purification. To purify the GST fusion proteins, cells were grown in 2 liters of LB broth with 100 µg/ml ampicillin at 37°C with shaking at 250 rpm until the optical density at 600 nm (OD₆₀₀) reached 0.8. Expression was then induced by the addition of 1 mM IPTG (isopropyl-β-D-thiogalactopyranoside), and the culture was grown for 12 h at 25°C with shaking at 250 rpm. For CheA, the culture was induced at 37°C for 4 h. Cells were then centrifuged at 8,000 × g for 8 min and resuspended in Tris-buffered saline (TBS) (50 mM Tris, 150 mM NaCl [pH 7.5]) supplemented with 1% Triton X-100 and 1 mM dithiothreitol (DTT) for every 1 g of cell pellet. The cells were then disrupted by sonication (5 10-s pulses). The supernatants were clarified by two rounds of centrifugation (9,000 × g for 15 min and 40,000 × g for 40 min) and loaded onto 5-ml GSTrap columns prewashed with 10 column volumes of TBS. Protein-bound columns were then washed with at least 15 volumes of TBS, and GST-tagged proteins were eluted using 10 ml glutathione elution buffer (GEB) (50 mM Tris, 5 mM glutathione [pH 8]). To remove the GST tag, the purified proteins were cleaved by PreScission protease, as specified by the supplier (Amersham Biosciences), and applied to another 5-ml GSTrap column. The flowthrough was collected and concentrated to approximately 5 ml using a cellulose ultrafiltration membrane (Millipore) in an Amicon ultrafiltration cell. Finally, the purified proteins were dialyzed in TKMD buffer (50 mM Tris, 50 mM KCl, 5 mM MgCl₂, 0.1 mM DTT [pH 8]), and aliquots were stored at -80°C.

E. coli BL21(DE3) cells harboring the His₆-tagged expression plasmids were grown in 2 liters of LB medium supplemented with 30 µg/ml kanamycin at 37°C with shaking at 250 rpm until the A₆₀₀ reached

0.7. Expression was then induced by the addition of 1 mM IPTG, and the cultures were grown for 12 h at 25°C. Cells were harvested by centrifugation at $7,000 \times g$ at 4°C for 10 min. Cells harboring HemAT_N were resuspended in lysis buffer (50 mM NaH₂PO₄, 300 mM NaCl, 10 mM imidazole [pH 8]) and sonicated (5 10-s pulses). Cell debris was removed by centrifugation at $12,000 \times g$ for 1 h. The dark-red supernatant containing HemAT_N was loaded onto a 5-ml GE HisTrap column prewashed with NiSO₄ and binding buffer (50 mM NaH₂PO₄, 300 mM NaCl, 20 mM imidazole [pH 8]). The protein-bound column was then washed with binding buffer, and proteins were eluted with elution buffer (50 mM NaH₂PO₄, 300 mM NaCl, 250 mM imidazole [pH 8]). The collected HemAT_N protein samples were concentrated using an Amicon ultrafiltration cell (Millipore) and dialyzed into dialysis buffer (50 mM Tris, 300 mM NaCl [pH 8]) at 4°C, and aliquots were stored at -80°C.

The McpB_C, McpB_C-A431S, McpA_C, and HemAT_S proteins were purified under denaturing conditions. Briefly, cells were induced and grown as described above. Cells were then resuspended in buffer B (8 M urea, 0.1 M NaH₂PO₄, 0.01 M Tris [pH 8]) with 1% Triton X-100 and 1 mM DTT for every 1 g of cell pellet and incubated at room temperature for 1 h. The cell suspension was clarified by centrifugation at $40,000 \times g$ for 1 h. The cell lysates were loaded onto a 5-ml GE Hi-Trap chelating column charged with 0.1 M NiSO₄ and washed with buffer B and buffer C (buffer B at pH 6.3). The fusion proteins were eluted from the column with 25 ml elution buffer E (buffer B at pH 4.5). Proteins were refolded by dialysis in phosphate-buffered saline (PBS) (10 mM Na₂HPO₄, 1.8 mM KH₂PO₄, 137 mM NaCl, 2.7 mM KCl [pH 7.4]) at 4°C, and aliquots were stored at -80°C. The proper folding of purified proteins was verified by circular dichroism (CD) spectroscopy. The concentrations of all purified proteins were quantified by a Pierce bicinchoninic acid (BCA) protein assay kit. SDS-PAGE images of the purified recombinant chemoreceptor proteins are provided in Data Set S1.

Capillary assay for chemotaxis. The capillary assay was performed as described previously (73). Briefly, cells were grown for 16 h at 30°C on TBAB plates. The cells were then scraped from the plates and resuspended to an OD₆₀₀ of 0.03 in 5 ml CAMM supplemented with 50 μg/ml histidine, 50 μg/ml methionine, 50 μg/ml tryptophan, 20 mM sorbitol, and 2% TB. The cultures were grown to an OD₆₀₀ of 0.4 to 0.45 at 37°C with shaking at 250 rpm. At this point, 50 μl of GL solution (5% [vol/vol] glycerol and 0.5 M sodium lactate) was added, and cells were incubated for another 15 min (at 37°C with shaking at 250 rpm). The cells were then washed twice with chemotaxis buffer and incubated for an additional 25 min (at 37°C with shaking at 250 rpm) to ensure that the cells were motile. The cells were then diluted to an OD₆₀₀ of 0.001 in chemotaxis buffer and aliquoted into 0.3-ml ponds on a slide warmer at 37°C, and closed-end capillary tubes filled with alcohol solutions or an asparagine solution (3.16 μM) prepared in the same chemotaxis buffer were inserted. After 30 min, cells in the capillaries were harvested, transferred to 3 ml of top agar (1% tryptone, 0.8% NaCl, 0.8% agar, and 0.5 mM EDTA), and plated onto TB agar (TB and 1.5% agar) plates. These plates were incubated for 16 h at 37°C, and colonies were counted. Experiments were performed in triplicate each day and repeated on three different days.

Cell growth. Cell density was measured as the optical absorbance at 600 nm. Briefly, *B. subtilis* 168 was first grown for 16 h at 30°C on a TBAB plate. For growth experiments in minimal medium, the cells were first scraped from the TBAB plate and then resuspended to an OD₆₀₀ of 0.03 in 50 ml CAMM supplemented with 50 μg/ml tryptophan and 5 g/liter glucose and grown at 37°C with shaking at 250 rpm. At an OD₆₀₀ of 0.8, the cells were diluted 1:20 (vol/vol) into 50 ml CAMM containing 50 μg/ml tryptophan supplemented with 0.01 M ethanol, 0.1 M ethanol, or 5 g/liter glucose (positive control) and grown for 24 h at 37°C with shaking at 250 rpm. For growth experiments in rich medium, cell cultures starting at an OD₆₀₀ of 0.03 were grown to an OD₆₀₀ of 0.4 at 37°C with shaking at 250 rpm in 50 ml LB medium. At this point, cell cultures were supplemented with 0.01 M, 0.1 M, or 1.0 M ethanol and grown for another 5 h at 37°C with shaking at 250 rpm. All growth experiments were performed in triplicate.

Ethanol utilization experiments. Ethanol concentrations were measured using a Shimadzu high-performance liquid chromatography system equipped with a RID-10A refractive index detector, an Aminex HPX-87H carbohydrate analysis column (Bio-Rad Laboratories), and a cation H micro-guard cartridge (Bio-Rad Laboratories). The column and guard cartridge were kept at 65°C, and 0.5 mM H₂SO₄ was used a mobile phase at a constant flow rate of 0.6 ml/min. Prior to measurements, cells in culture samples were pelleted, and the resulting supernatant was passed through a 0.22-μm polyethersulfone syringe filter. Peaks were identified and quantified by retention time comparison to the standards.

Alcohol dehydrogenase activity measurement. *B. subtilis* OI1085 was first grown for 16 h at 30°C on a TBAB plate. For aerobic growth, the cells were then scraped from the TBAB plate; resuspended to an OD₆₀₀ of 0.03 in 5 ml CAMM supplemented with 50 μg/ml histidine, 50 μg/ml methionine, 50 μg/ml tryptophan, 20 mM sorbitol, and 2% TB; and grown at 37°C with vigorous shaking at 250 rpm. For anaerobic growth, however, cells were cultured starting at an OD₆₀₀ of 0.03 in a sealed bottle filled to the top without agitation in CAMM supplemented with 1% glucose and a mixture of all 20 amino acids at 50 μg/ml (29). For *E. coli* cultures, the cells (MG1655) were grown in M9 medium supplemented with 0.4% glucose at 37°C in sealed bottles filled to the top without agitation for anaerobic growth and in flasks with shaking at 250 rpm for aerobic growth (31). All cell cultures were grown to stationary phase prior to sonication (7 10-s pulses), and soluble cell extracts were obtained by centrifugation ($7,000 \times g$ at 4°C for 10 min). Alcohol dehydrogenase enzyme assays were performed as described previously (74). Briefly, the assay reaction mixtures were prepared with 22 mM sodium pyrophosphate (pH 8.8), 0.3 mM sodium phosphate, 7.5 mM β-NAD, 0.003% (wt/vol) bovine serum albumin, 1.6% (vol/vol) of the desired cell lysate, and 3.2% (vol/vol) ethanol in a 200-μl reaction volume. Next, the reduction of NAD⁺ to NADH was recorded at 340 nm using a Shimadzu UV-1800 spectrophotometer. One unit of alcohol dehydrogenase activity is defined as the amount of enzyme that converts 1 μmol of ethanol to acetaldehyde per min at pH 8.8 at 25°C.

Antimicrobial diffusion assay. The antifungal activities of the *B. subtilis* strains were assayed using the disc diffusion method as described previously (75). Briefly, *S. cerevisiae* CEN.PK113-7D was grown in YPD rich medium for 24 h at 30°C with shaking at 200 rpm. A total of 0.1% (vol/vol) of the yeast culture was mixed with YPD top agar (YPD medium with 0.8% agar) and spread on top of a YPD plate (YPD medium with 2% agar). Once the top yeast layer was solidified, 10-mm filter paper (Whatman filter paper, grade 1) discs loaded with supernatants from *B. subtilis* strains grown overnight in LB medium at 37°C were placed on top of the yeast layer. As negative controls, separate discs were loaded with LB broth and water. The plate was incubated at 30°C for another 24 h and then imaged. A zone of inhibition around the discs indicated antifungal activity.

Preparation of bacterial membranes. Cells were grown for 16 h at 30°C on TBAB plates. The cells were then scraped from the plates and resuspended to an OD₆₀₀ of 0.03 in 50 ml CAMM supplemented with 50 µg/ml histidine, 50 µg/ml methionine, 50 µg/ml tryptophan, 20 mM sorbitol, and 2% TB. The cells were grown at 37°C with aeration until they reached mid-exponential phase. The cells were then diluted 1:10 (vol/vol) into 50 ml CAMM and grown until mid-exponential phase. The cells were again diluted to an OD₆₀₀ of 0.01 in 50 ml medium and grown until mid-exponential phase. Finally, the cultures were diluted 1:10 (vol/vol) into multiple flasks containing 50 ml medium and grown with shaking at 37°C until an OD₆₀₀ of 0.6 was reached. The cells were then harvested by centrifugation at 9,900 × *g* for 15 min and washed 3 times with 1 M KCl to remove extracellular proteases. Cells were resuspended in sonication buffer plus (10 mM potassium phosphate [pH 7], 10 mM MgCl₂, 1 mM EDTA, 0.3 mM DTT, 20 mM KCl, 1 mM glutamate, 2 mM phenylmethanesulfonyl fluoride, and 20% glycerol). EDTA and phenylmethanesulfonyl fluoride were added as protease inhibitors. Cells were sonicated, and the cell debris was removed by centrifugation at 17,600 × *g* at 4°C for 15 min. Bacterial membranes were removed by centrifugation at 120,000 × *g* for 2 h at 4°C in a Beckman 70 Ti rotor. Pelleted membranes were resuspended in MT buffer (10 mM potassium phosphate [pH 7], 1 mM MgCl₂, 0.1 mM EDTA, and 1 mM 2-mercaptoethanol) and homogenized using a glass-Teflon homogenizer, followed by another centrifugation step at 120,000 × *g* for 2 h at 4°C. This step was repeated once more. Finally, the membranes were homogenized in MT buffer at a concentration of 32 mg/ml and stored in small aliquots at –80°C.

In vitro assay for receptor-coupled kinase activity. Reaction mixtures consisted of purified *B. subtilis* membranes expressing McpB or HemAT as the sole chemoreceptor and purified CheW, CheA, and CheD prepared in buffer (50 mM Tris, 50 mM KCl, 5 mM MgCl₂ [pH 7.5]) at the following concentrations: 6 µM chemoreceptor, 2 µM CheW, 2 µM CheA kinase, and 2 µM CheD. Ethanol was then added to the mixture at different final concentrations in a 20-µl reaction volume. As a negative control, only buffer was added. Reaction mixtures were then preincubated at 23°C for 1 h to permit the formation of the chemoreceptor-kinase complex. CheA autophosphorylation was initiated by the addition of [γ -³²P]ATP (4,000 to 8,000 cpm/pmol) to a final concentration of 0.1 mM. Five-microliter aliquots were quenched at 15 s by mixing the reaction mixtures with 15 µl of 2× Laemmli sample buffer containing 25 mM EDTA at room temperature, essentially fixing the level of phosphor-CheA. Initial phosphor-CheA formation rates were analyzed using 12% SDS-PAGE gels. Gels were dried immediately after electrophoresis, and phosphor-CheA was quantified by phosphorimaging (Molecular Dynamics) and ImageJ (76).

Circular dichroism spectroscopy. Far-UV CD spectra were measured on a Jasco J-720 spectropolarimeter (Japan Spectroscopic Co., Inc., Tokyo, Japan) with a cuvette with a path length of 0.1 cm. Prior to measurements, protein samples were dialyzed into 10 mM sodium phosphate buffer (pH 8) and diluted to 2.5 µM. Spectral measurements were carried out in triplicate using a scanning rate of 50 nm/min and a 0.1-nm step size with 5 accumulations per sample. A buffer-only control sample was used for baseline correction, and curves were smoothed according to the Savitzky-Golay algorithm (77). Structural analysis was done using BeStSel (78).

UV-visible spectral measurements. All UV spectral measurements were performed on a Shimadzu UV-1800 spectrophotometer. The UV spectra of the oxygenated sensing domain of the HemAT (HemAT_N) protein were measured under aerobic conditions. To measure the UV spectra of HemAT_N in the presence of ethanol, protein samples were first deoxygenated by adding a few grains of sodium dithionite in a glove box. Sodium dithionite-reduced protein samples were then titrated with different doses of ethanol in sealed quartz cuvettes, and the UV spectra (200 nm to 600 nm) of these samples were immediately recorded in the spectrophotometer.

Saturation transfer difference nuclear magnetic resonance spectroscopy. All nuclear magnetic resonance (NMR) spectroscopy measurements were performed on a Varian VNMR5 instrument at 750 MHz with a 5-mm Varian HCN probe at 298 K without sample spinning. Prior to measurements, protein samples were buffer exchanged into PBS (50 mM KH₂PO₄, 20 mM NaCl [pH 7.4]) in D₂O using Micro Bio-Spin columns with Bio-Gel P-6 (Bio-Rad Laboratories, Hercules, CA, USA). To avoid aggregation, HemAT_N protein was buffer exchanged into modified PBS (50 mM KH₂PO₄, 300 mM NaCl [pH 8.0]) containing 10% D₂O. Protein samples at 50 µM were then mixed with the alcohol (final concentration of 3 mM) in a 500-µl solution. ¹H spectra were obtained from 32 scans with a 90° pulse and a 2-s relaxation delay. In saturation transfer difference NMR (STD-NMR) experiments, the protein samples were selectively saturated at 2.15 ppm with a train of Gaussian pulses of a 50-ms duration with a 0.1-ms delay and a 5-s relaxation delay for a total saturation time of 3 s and 2,048 scans. Off-resonance irradiation was applied at 30 ppm. A trim pulse of 50 ms was used to reduce protein background. In the case of HemAT_N, the protein sample was saturated at 7.06 ppm, and 256 scans were used to obtain spectra. All STD spectra were obtained by internal subtraction via phase cycling after a block size of 8 to reduce artifacts resulting from temperature variation and magnet instability. Control experiments were performed on samples containing only the alcohol without protein. All areas were calculated using MNova V14.1 (by Mestrelab Chemistry Solutions) in stacked mode.

Structural analysis. Domains of the McpB, McpA, TlpA, and TlpB chemoreceptors from *B. subtilis* were predicted using the phmmer search engine on the HMMER Web server using the UniProt reference proteome database with default sequence E value thresholds (79). The amino acid sequences of the cytoplasmic signaling domains were then manually obtained based on previous large-scale alignment results (10). To identify the three structural subdomains of the cytoplasmic signaling domain, the sequences were then aligned with the amino acid sequences of the corresponding domains from the Tar, Tsr, Trg, and Tap chemoreceptors of *E. coli* using MUSCLE (80) with default parameter values. Pairwise amino acid sequence alignments between the protein pairs (McpA-McpB, McpA-HemAT, and HemAT-YfmS) for chimeric receptor analysis were performed using EMBOSS Water (81). A homology model of the cytoplasmic signaling domain of the McpB dimer (residues 352 to 662) was constructed in Modeller (v-9.23) (82) using the *Thermotoga maritima* Tm113 chemoreceptor (PDB accession number 2CH7) as the template (83). Side chain conformations were refined using SCWRL4 (84), and the entire structural model was subsequently refined using the YASARA energy minimization server (85). The resulting Ramachandran plots were verified using Procheck (86). The crystal structure of the HemAT sensing domain from *B. subtilis* (PDB accession number 1OR6) (40) was used for visualization. Visualization of all structures was accomplished using the VMD software package (v-1.9.3) (87).

Receptor-ligand *in silico* docking experiment. The putative binding sites for ethanol were determined using Autodock (v-4.0) (88). Briefly, hydrogen atoms were first added to the McpB cytoplasmic signaling domain dimer model, and the number of torsional degrees of freedom for ethanol was set at 1. Autogrid was then used to adjust the position of grid boxes (60 by 60 by 60 points with 0.375-Å spacing for each box) on the ethanol-sensing region (residues 390 to 435). Finally, the Lamarckian genetic algorithm was employed to obtain the best docking site configurations.

Molecular dynamics simulations. All-atom molecular dynamics simulations were conducted using NAMD 2.13 (89) and the CHARMM36 force field (90). Simulations were carried out using the NPT ensemble (pressure of 1 atm and temperature of 310 K) with values for general simulation parameters as previously described (91). The McpB cytoplasmic dimer model was solvated with TIP3P (transferable intermolecular potential with 3 points) water and 150 mM NaCl using VMD (87), and 165 ethanol molecules (0.316 M) were randomly placed within the simulation box using the gmx insert-molecules tool. A copy of the system that included the A431S mutation was created, and both the wild-type and mutant McpB-ethanol systems were subjected to conjugate gradient energy minimization (2,000 steps), followed by a 10-ns equilibration simulation with protein backbone restraints and 3 600-ns unrestrained production simulations.

Molecular dynamics simulation analysis. Density maps representing the average ethanol occupancy were computed using the VolMap plug-in in VMD with default settings and averaging over each production simulation for the wild-type and A431S mutant McpB-ethanol systems. To highlight unique binding sites between the two maps, a difference map was computed by subtracting the A431S map from the wild-type map using VMD's volutil plug-in and removing smaller volumes resulting from slight irregularities in overlapping sites using the "hide dust" feature in UCSF Chimera. All densities are visualized at an isovalue of 0.03 except for the difference map, which used an isovalue of 0.015. Protein-ethanol coordination was computed by measuring the minimum distance between nonhydrogen atoms in each residue and the nearest ethanol molecule; if this distance was less than 4 Å, the pair was considered to be in contact. Average coordination values were computed for each residue in the wild-type and A431S mutant McpB-ethanol systems by averaging over all three production simulations at 200-ps intervals. Percent changes were obtained by subtracting the values obtained in the latter from those obtained in the former. Knobs-in-holes packing within the McpB cytoplasmic signaling domain was analyzed using the program SOCKET (92) with a packing cutoff of 7.8 Å (93). For each production simulation, knobs-in-holes packing was assessed at 2-ns intervals over the course of the trajectory, not including the first 100 ns to allow for packing changes resulting from equilibration or the A431S mutation. The occupancy of a particular knob-in-hole interaction over a given simulation was taken as the number of intervals in which it was identified by SOCKET divided by the total number of intervals analyzed in the simulation. The reported knobs-in-holes occupancies were averaged over both McpB monomers and all three production simulations for each McpB-ethanol system; error bars denote 1 standard deviation from the mean.

Simulation of ethanol diffusion in the capillary assay. The spatiotemporal evolution of ethanol (*C*) in the capillary assay was modeled using Fick's second-law equation with Neumann (no-flux) boundary conditions shown in the following equation: $\partial C/\partial t = D\Delta C$. The initial ethanol concentrations were set to 50 mM in the capillary and 0 mM in the pond. The ethanol diffusion coefficient (*D*) was assumed to be 1.23×10^{-3} mm²/s (94). The above-described partial differential equation was solved using the finite-element method with the help of FEniCS (v-2019.1.0), an open-source computing platform (95). Briefly, the computation domain consists of the capillary and the proximal region near the mouth of the capillary in the pond. The capillary was modeled as a 10-mm-long cylinder with a diameter of 0.2 mm attached to an 8-mm-long cylinder with a diameter of 4 mm. Gmsh (v-4.5.2) (96) was used to generate the three-dimensional finite-element mesh, and the XML file of the resulting mesh was produced using the meshio-convert tool available from FEniCS. The implicit Euler method was employed for time integration with a step size of $\Delta t = 1$ s. A custom Python script was generated for solving the finite-element problem.

Data availability. Raw data for all experiments except STD-NMR are provided in Data Set S1 in the supplemental material. Raw data for the STD-NMR experiments are available upon request. The Python script for diffusion simulation is provided at <https://github.com/paymantohidifar/alccoholtaxi>.

SUPPLEMENTAL MATERIAL

Supplemental material is available online only.

FIG S1, TIF file, 1 MB.

FIG S2, TIF file, 2.9 MB.

FIG S3, TIF file, 2 MB.

FIG S4, TIF file, 0.5 MB.

FIG S5, TIF file, 2.4 MB.

FIG S6, TIF file, 1.3 MB.

FIG S7, TIF file, 0.6 MB.

TABLE S1, PDF file, 0.02 MB.

TABLE S2, PDF file, 0.1 MB.

DATA SET S1, XLSX file, 0.3 MB.

ACKNOWLEDGMENTS

We thank Jodi A. Hadden-Perilla for discussions surrounding the use of SOCKET. We also thank Lingyang Zhu, Dean Olson, and the SCS NMR laboratory at the University of Illinois at Urbana-Champaign for valuable inputs and help with NMR measurements and Ahmed Hetta and Isaac Cann for help with CD spectroscopy experiments.

This work was partially funded by National Institutes of Health grant GM054365 and by the University of Illinois through the Robert W. Schaefer Faculty Scholar Fund.

REFERENCES

- Adler J. 1966. Chemotaxis in bacteria. *Science* 153:708–716. <https://doi.org/10.1126/science.153.3737.708>.
- Ortega A, Zhulin IB, Krell T. 2017. Sensory repertoire of bacterial chemoreceptors. *Microbiol Mol Biol Rev* 81:e00033-17. <https://doi.org/10.1128/MMBR.00033-17>.
- Rao CV, Ordal GW. 2009. The molecular basis of excitation and adaptation during chemotactic sensory transduction in bacteria. *Contrib Microbiol* 16:33–64. <https://doi.org/10.1159/000219372>.
- Rao CV, Glekas GD, Ordal GW. 2008. The three adaptation systems of *Bacillus subtilis* chemotaxis. *Trends Microbiol* 16:480–487. <https://doi.org/10.1016/j.tim.2008.07.003>.
- Kristich CJ, Glekas GD, Ordal GW. 2003. The conserved cytoplasmic module of the transmembrane chemoreceptor McpC mediates carbohydrate chemotaxis in *Bacillus subtilis*. *Mol Microbiol* 47:1353–1366. <https://doi.org/10.1046/j.1365-2958.2003.03375.x>.
- Neumann S, Grosse K, Sourjik V. 2012. Chemotactic signaling via carbohydrate phosphotransferase systems in *Escherichia coli*. *Proc Natl Acad Sci U S A* 109:12159–12164. <https://doi.org/10.1073/pnas.1205307109>.
- Umehura T, Matsumoto Y, Ohnishi K, Homma M, Kawagishi I. 2002. Sensing of cytoplasmic pH by bacterial chemoreceptors involves the linker region that connects the membrane-spanning and the signal-modulating helices. *J Biol Chem* 277:1593–1598. <https://doi.org/10.1074/jbc.M109930200>.
- Bi S, Jin F, Sourjik V. 2018. Inverted signaling by bacterial chemotaxis receptors. *Nat Commun* 9:2927. <https://doi.org/10.1038/s41467-018-05335-w>.
- Vaknin A, Berg HC. 2006. Osmotic stress mechanically perturbs chemoreceptors in *Escherichia coli*. *Proc Natl Acad Sci U S A* 103:592–596. <https://doi.org/10.1073/pnas.0510047103>.
- Alexander RP, Zhulin IB. 2007. Evolutionary genomics reveals conserved structural determinants of signaling and adaptation in microbial chemoreceptors. *Proc Natl Acad Sci U S A* 104:2885–2890. <https://doi.org/10.1073/pnas.0609359104>.
- Dombek KM, Ingram LO. 1986. Determination of the intracellular concentration of ethanol in *Saccharomyces cerevisiae* during fermentation. *Appl Environ Microbiol* 51:197–200. <https://doi.org/10.1128/AEM.51.1.197-200.1986>.
- Osman YA, Ingram LO. 1985. Mechanism of ethanol inhibition of fermentation in *Zymomonas mobilis* CP4. *J Bacteriol* 164:173–180. <https://doi.org/10.1128/JB.164.1.173-180.1985>.
- Schoberth SM, Chapman BE, Kuchel PW, Wittig RM, Grotendorst J, Jansen P, DeGraff AA. 1996. Ethanol transport in *Zymomonas mobilis* measured by using in vivo nuclear magnetic resonance spin transfer. *J Bacteriol* 178:1756–1761. <https://doi.org/10.1128/jb.178.6.1756-1761.1996>.
- Stein WD. 1986. Transport and diffusion across cell membranes. Academic Press, Inc, San Diego, CA. <https://doi.org/10.1016/b978-0-12-664660-3.X5001-7>.
- Stock JB, Rauch B, Roseman S. 1977. Periplasmic space in *Salmonella typhimurium* and *Escherichia coli*. *J Biol Chem* 252:7850–7861.
- Yang NJ, Hinner MJ. 2015. Getting across the cell membrane: an overview for small molecules, peptides, and proteins. *Methods Mol Biol* 1266:29–53. https://doi.org/10.1007/978-1-4939-2272-7_3.
- Stewart GG, Panchal CJ, Russell I, Sills AM. 1983. Biology of ethanol-producing microorganisms. *Crit Rev Biotechnol* 1:161–188. <https://doi.org/10.3109/07388558309077977>.
- Glekas GD, Foster RM, Cates JR, Estrella JA, Wawrzyniak MJ, Rao CV, Ordal GW. 2010. A PAS domain binds asparagine in the chemotaxis receptor McpB in *Bacillus subtilis*. *J Biol Chem* 285:1870–1878. <https://doi.org/10.1074/jbc.M109.072108>.
- Glekas GD, Mulhern BJ, Kroc A, Duelfer KA, Lei V, Rao CV, Ordal GW. 2012. The *Bacillus subtilis* chemoreceptor McpC senses multiple ligands using two discrete mechanisms. *J Biol Chem* 287:39412–39418. <https://doi.org/10.1074/jbc.M112.413518>.
- Ordal GW, Villani DP, Gibson KJ. 1977. Amino acid chemoreceptors of *Bacillus subtilis*. *J Bacteriol* 129:156–165. <https://doi.org/10.1128/JB.129.1.156-165.1977>.
- Bohin JP, Rigomier D, Schaeffer P. 1976. Ethanol sensitivity of sporulation in *Bacillus subtilis*: a new tool for the analysis of the sporulation process. *J Bacteriol* 127:934–940. <https://doi.org/10.1128/JB.127.2.934-940.1976>.
- Walukiewicz HE, Tohidifar P, Ordal GW, Rao CV. 2014. Interactions among the three adaptation systems of *Bacillus subtilis* chemotaxis as revealed by an in vitro receptor-kinase assay. *Mol Microbiol* 93:1104–1118. <https://doi.org/10.1111/mmi.12721>.
- Cannistraro VJ, Glekas GD, Rao CV, Ordal GW. 2011. Cellular stoichiometry of the chemotaxis proteins in *Bacillus subtilis*. *J Bacteriol* 193:3220–3227. <https://doi.org/10.1128/JB.01255-10>.
- Hou S, Larsen RW, Boudko D, Riley CW, Karatan E, Zimmer M, Ordal GW, Alam M. 2000. Myoglobin-like aerotaxis transducers in *Archaea* and *Bacteria*. *Nature* 403:540–544. <https://doi.org/10.1038/35000570>.
- Tohidifar P, Plutz MJ, Ordal GW, Rao CV. 2020. The mechanism of bidirectional pH taxis in *Bacillus subtilis*. *J Bacteriol* 202:e00491-19. <https://doi.org/10.1128/JB.00491-19>.
- Reid MF, Fewson CA. 1994. Molecular characterization of microbial alcohol dehydrogenases. *Crit Rev Microbiol* 20:13–56. <https://doi.org/10.3109/10408419409113545>.
- Zhang X, Hughes JG, Subuyuj GA, Ditty JL, Parales RE. 2019. Chemotaxis of *Pseudomonas putida* F1 to alcohols is mediated by the carboxylic acid

- receptor McFP. *Appl Environ Microbiol* 85:e01625-19. <https://doi.org/10.1128/AEM.01625-19>.
28. Alexandre G. 2010. Coupling metabolism and chemotaxis-dependent behaviours by energy taxis receptors. *Microbiology* 156:2283–2293. <https://doi.org/10.1099/mic.0.039214-0>.
 29. Nakano MM, Dailly YP, Zuber P, Clark DP. 1997. Characterization of anaerobic fermentative growth of *Bacillus subtilis*: identification of fermentation end products and genes required for growth. *J Bacteriol* 179:6749–6755. <https://doi.org/10.1128/jb.179.21.6749-6755.1997>.
 30. Nakano MM, Hulett FM. 1997. Adaptation of *Bacillus subtilis* to oxygen limitation. *FEMS Microbiol Lett* 157:1–7. <https://doi.org/10.1111/j.1574-6968.1997.tb12744.x>.
 31. Leonardo MR, Cunningham PR, Clark DP. 1993. Anaerobic regulation of the *adhE* gene, encoding the fermentative alcohol dehydrogenase of *Escherichia coli*. *J Bacteriol* 175:870–878. <https://doi.org/10.1128/jb.175.3.870-878.1993>.
 32. Walukiewicz HE, Ordal GW, Rao CV. 2018. In vitro assay for measuring receptor-kinase activity in the *Bacillus subtilis* chemotaxis pathway. *Methods Mol Biol* 1729:95–105. https://doi.org/10.1007/978-1-4939-7577-8_10.
 33. Bi S, Pollard AM, Yang Y, Jin F, Sourjik V. 2016. Engineering hybrid chemotaxis receptors in bacteria. *ACS Synth Biol* 5:989–1001. <https://doi.org/10.1021/acssynbio.6b00053>.
 34. Weerasuriya S, Schneider BM, Manson MD. 1998. Chimeric chemoreceptors in *Escherichia coli*: signaling properties of Tar-Tap and Tap-Tar hybrids. *J Bacteriol* 180:914–920. <https://doi.org/10.1128/JB.180.4.914-920.1998>.
 35. Rahman H, King RM, Shewell LK, Semchenko EA, Hartley-Tassell LE, Wilson JC, Day CJ, Korolik V. 2014. Characterisation of a multi-ligand binding chemoreceptor CcmL (Tlp3) of *Campylobacter jejuni*. *PLoS Pathog* 10:e1003822. <https://doi.org/10.1371/journal.ppat.1003822>.
 36. Mayer M, Meyer B. 1999. Characterization of ligand binding by saturation transfer difference NMR spectroscopy. *Angew Chem Int Ed Engl* 38:1784–1788. [https://doi.org/10.1002/\(SICI\)1521-3773\(19990614\)38:12<1784::AID-ANIE1784>3.0.CO;2-Q](https://doi.org/10.1002/(SICI)1521-3773(19990614)38:12<1784::AID-ANIE1784>3.0.CO;2-Q).
 37. Mayer M, Meyer B. 2001. Group epitope mapping by saturation transfer difference NMR to identify segments of a ligand in direct contact with a protein receptor. *J Am Chem Soc* 123:6108–6117. <https://doi.org/10.1021/ja0100120>.
 38. Cala O, Krimm I. 2015. Ligand-orientation based fragment selection in STD NMR screening. *J Med Chem* 58:8739–8742. <https://doi.org/10.1021/acs.jmedchem.5b01114>.
 39. Viegas A, Manso J, Nobrega FL, Cabrita EJ. 2011. Saturation-transfer difference (STD) NMR: a simple and fast method for ligand screening and characterization of protein binding. *J Chem Educ* 88:990–994. <https://doi.org/10.1021/ed101169t>.
 40. Zhang W, Phillips GN, Jr. 2003. Structure of the oxygen sensor in *Bacillus subtilis*: signal transduction of chemotaxis by control of symmetry. *Structure* 11:1097–1110. [https://doi.org/10.1016/S0969-2126\(03\)00169-2](https://doi.org/10.1016/S0969-2126(03)00169-2).
 41. Zhang W, Olson JS, Phillips GN, Jr. 2005. Biophysical and kinetic characterization of HemAT, an aerotaxis receptor from *Bacillus subtilis*. *Biophys J* 88:2801–2814. <https://doi.org/10.1529/biophysj.104.047936>.
 42. Hou S, Freitas T, Larsen RW, Piatibratov M, Sivozhelozov V, Yamamoto A, Meleshkevitch EA, Zimmer M, Ordal GW, Alam M. 2001. Globin-coupled sensors: a class of heme-containing sensors in Archaea and Bacteria. *Proc Natl Acad Sci U S A* 98:9353–9358. <https://doi.org/10.1073/pnas.161185598>.
 43. Aono S, Kato T, Matsuki M, Nakajima H, Ohta T, Uchida T, Kitagawa T. 2002. Resonance Raman and ligand binding studies of the oxygen-sensing signal transducer protein HemAT from *Bacillus subtilis*. *J Biol Chem* 277:13528–13538. <https://doi.org/10.1074/jbc.M112256200>.
 44. Mohd Azhar SH, Abdulla R, Jambo SA, Marbawi H, Gansau JA, Mohd Faik AA, Rodrigues KF. 2017. Yeasts in sustainable bioethanol production: a review. *Biochem Biophys Rep* 10:52–61. <https://doi.org/10.1016/j.bbrep.2017.03.003>.
 45. Russo F, Cabrita M, Feio SS, Moiteiro C, Tavares R, Marcelo-Curto MJ, Roseiro JC. 2002. Antifungal activity of *Bacillus* species and *Pseudomonas aeruginosa* against filamentous fungi and yeasts, p 249–253. In Rauter AP, Palma FB, Justino J, Araújo ME, dos Santos SP (ed), *Natural products in the new millennium: prospects and industrial application. Proceedings of the Phytochemical Society of Europe*, vol 47. Springer, Dordrecht, Netherlands. https://doi.org/10.1007/978-94-015-9876-7_26.
 46. Leifert C, Li H, Chidburee S, Hampson S, Workman S, Sigee D, Epton HA, Harbour A. 1995. Antibiotic production and biocontrol activity by *Bacillus subtilis* CL27 and *Bacillus pumilus* CL45. *J Appl Bacteriol* 78:97–108. <https://doi.org/10.1111/j.1365-2672.1995.tb02829.x>.
 47. Podile AR, Prakash AP. 1996. Lysis and biological control of *Aspergillus niger* by *Bacillus subtilis* AF 1. *Can J Microbiol* 42:533–538. <https://doi.org/10.1139/m96-072>.
 48. Ohimain EI. 2016. Methanol contamination in traditionally fermented alcoholic beverages: the microbial dimension. *Springerplus* 5:1607. <https://doi.org/10.1186/s40064-016-3303-1>.
 49. Yasueda H, Kawahara Y, Sugimoto S. 1999. *Bacillus subtilis* *yckG* and *yckF* encode two key enzymes of the ribulose monophosphate pathway used by methylotrophs, and *yckH* is required for their expression. *J Bacteriol* 181:7154–7160. <https://doi.org/10.1128/JB.181.23.7154-7160.1999>.
 50. Yang YM, Pollard A, Hofler C, Poschet G, Wirtz M, Hell R, Sourjik V. 2015. Relation between chemotaxis and consumption of amino acids in bacteria. *Mol Microbiol* 96:1272–1282. <https://doi.org/10.1111/mmi.13006>.
 51. Allard-Massicotte R, Tessier L, Lecuyer F, Lakshmanan V, Lucier JF, Garneau D, Caudwell L, Vlamakis H, Bais HP, Beauregard PB. 2016. *Bacillus subtilis* early colonization of *Arabidopsis thaliana* roots involves multiple chemotaxis receptors. *mBio* 7:e01664-16. <https://doi.org/10.1128/mBio.01664-16>.
 52. Tso WW, Adler J. 1974. Negative chemotaxis in *Escherichia coli*. *J Bacteriol* 118:560–576. <https://doi.org/10.1128/JB.118.2.560-576.1974>.
 53. Oku S, Hida A, Mattana T, Tajima T, Nakashimada Y, Kato J. 2017. Involvement of many chemotaxis sensors in negative chemotaxis to ethanol in *Ralstonia pseudosolanacearum* Ps29. *Microbiology* 163:1880–1889. <https://doi.org/10.1099/mic.0.000574>.
 54. Harris RA, Trudell JR, Mihic SJ. 2008. Ethanol's molecular targets. *Sci Signal* 1:re7. <https://doi.org/10.1126/scisignal.128re7>.
 55. Dudley R. 2004. Ethanol, fruit ripening, and the historical origins of human alcoholism in primate frugivory. *Integr Comp Biol* 44:315–323. <https://doi.org/10.1093/icb/44.4.315>.
 56. Alpi A, Beevers H. 1983. Effects of O₂ concentration on rice seedlings. *Plant Physiol* 71:30–34. <https://doi.org/10.1104/pp.71.1.30>.
 57. Setter T. 1994. Relationship between coleoptile elongation and alcoholic fermentation in rice exposed to anoxia. II. Cultivar differences. *Ann Bot* 74:273–279. <https://doi.org/10.1006/anbo.1994.1118>.
 58. Kato-Noguchi H, Kugimiya T. 2001. Effects of ethanol on growth of rice seedlings. *Plant Growth Regul* 35:93–96. <https://doi.org/10.1023/A:1013850707053>.
 59. Mihic SJ, Ye Q, Wick MJ, Koltchine VV, Krasowski MD, Finn SE, Mascia MP, Valenzuela CF, Hanson KK, Greenblatt EP, Harris RA, Harrison NL. 1997. Sites of alcohol and volatile anaesthetic action on GABA(A) and glycine receptors. *Nature* 389:385–389. <https://doi.org/10.1038/38738>.
 60. Taly A, Delarue M, Grutter T, Nilges M, Le Novère N, Corringer PJ, Changeux JP. 2005. Normal mode analysis suggests a quaternary twist model for the nicotinic receptor gating mechanism. *Biophys J* 88:3954–3965. <https://doi.org/10.1529/biophysj.104.050229>.
 61. Cheng MH, Cascio M, Coalson RD. 2007. Homology modeling and molecular dynamics simulations of the alpha1 glycine receptor reveals different states of the channel. *Proteins* 68:581–593. <https://doi.org/10.1002/prot.21435>.
 62. Ren H, Zhao Y, Wu M, Dwyer DS, Peoples RW. 2017. Two adjacent phenylalanines in the NMDA receptor GluN2A subunit M3 domain interactively regulate alcohol sensitivity and ion channel gating. *Neuropharmacology* 114:20–33. <https://doi.org/10.1016/j.neuropharm.2016.11.013>.
 63. Shahidullah M, Harris T, Germann MW, Covarrubias M. 2003. Molecular features of an alcohol binding site in a neuronal potassium channel. *Biochemistry* 42:11243–11252. <https://doi.org/10.1021/bi034738f>.
 64. Kruse SW, Zhao R, Smith DP, Jones DN. 2003. Structure of a specific alcohol-binding site defined by the odorant binding protein LUSH from *Drosophila melanogaster*. *Nat Struct Biol* 10:694–700. <https://doi.org/10.1038/nsb960>.
 65. Howard RJ, Murail S, Ondricek KE, Corringer PJ, Lindahl E, Trudell JR, Harris RA. 2011. Structural basis for alcohol modulation of a pentameric ligand-gated ion channel. *Proc Natl Acad Sci U S A* 108:12149–12154. <https://doi.org/10.1073/pnas.1104480108>.
 66. Dwyer DS, Bradley RJ. 2000. Chemical properties of alcohols and their protein binding sites. *Cell Mol Life Sci* 57:265–275. <https://doi.org/10.1007/PL00000689>.
 67. Khrustalev VV, Khrustaleva TA, Lelevich SV. 2017. Ethanol binding sites on proteins. *J Mol Graph Model* 78:187–194. <https://doi.org/10.1016/j.jmgm.2017.10.017>.
 68. Altenbuchner J. 2016. Editing of the *Bacillus subtilis* genome by the

- CRISPR-Cas9 system. *Appl Environ Microbiol* 82:5421–5427. <https://doi.org/10.1128/AEM.01453-16>.
69. Labun K, Montague TG, Krause M, Torres Cleuren YN, Tjeldnes H, Valen E. 2019. CHOPCHOP v3: expanding the CRISPR Web toolbox beyond genome editing. *Nucleic Acids Res* 47:W171–W174. <https://doi.org/10.1093/nar/gkz365>.
 70. Engler C, Kandzia R, Marillonnet S. 2008. A one pot, one step, precision cloning method with high throughput capability. *PLoS One* 3:e3647. <https://doi.org/10.1371/journal.pone.0003647>.
 71. Gibson DG, Young L, Chuang RY, Venter JC, Hutchison CA, III, Smith HO. 2009. Enzymatic assembly of DNA molecules up to several hundred kilobases. *Nat Methods* 6:343–345. <https://doi.org/10.1038/nmeth.1318>.
 72. Anagnostopoulos C, Spizizen J. 1961. Requirements for transformation in *Bacillus subtilis*. *J Bacteriol* 81:741–746. <https://doi.org/10.1128/JB.81.5.741-746.1961>.
 73. Ordal GW, Gibson KJ. 1977. Chemotaxis toward amino acids by *Bacillus subtilis*. *J Bacteriol* 129:151–155. <https://doi.org/10.1128/JB.129.1.151-155.1977>.
 74. Kagi JH, Vallee BL. 1960. The role of zinc in alcohol dehydrogenase. V. The effect of metal-binding agents on the structure of the yeast alcohol dehydrogenase molecule. *J Biol Chem* 235:3188–3192.
 75. Balouiri M, Sadiki M, Ibnouda SK. 2016. Methods for in vitro evaluating antimicrobial activity: a review. *J Pharm Anal* 6:71–79. <https://doi.org/10.1016/j.jpha.2015.11.005>.
 76. Schneider CA, Rasband WS, Eliceiri KW. 2012. NIH Image to ImageJ: 25 years of image analysis. *Nat Methods* 9:671–675. <https://doi.org/10.1038/nmeth.2089>.
 77. Savitzky A, Golay MJE. 1964. Smoothing and differentiation of data by simplified least squares procedures. *Anal Chem* 36:1627–1639. <https://doi.org/10.1021/ac60214a047>.
 78. Micsonai A, Wien F, Bulyaki E, Kun J, Moussong E, Lee YH, Goto Y, Refregiers M, Kardos J. 2018. BeStSel: a Web server for accurate protein secondary structure prediction and fold recognition from the circular dichroism spectra. *Nucleic Acids Res* 46:W315–W322. <https://doi.org/10.1093/nar/gky497>.
 79. Potter SC, Luciani A, Eddy SR, Park Y, Lopez R, Finn RD. 2018. HMMER Web server: 2018 update. *Nucleic Acids Res* 46:W200–W204. <https://doi.org/10.1093/nar/gky448>.
 80. Edgar RC. 2004. MUSCLE: a multiple sequence alignment method with reduced time and space complexity. *BMC Bioinformatics* 5:113. <https://doi.org/10.1186/1471-2105-5-113>.
 81. Rice P, Longden I, Bleasby A. 2000. EMBOSS: the European Molecular Biology Open Software Suite. *Trends Genet* 16:276–277. [https://doi.org/10.1016/s0168-9525\(00\)02024-2](https://doi.org/10.1016/s0168-9525(00)02024-2).
 82. Webb B, Sali A. 2016. Comparative protein structure modeling using MODELLER. *Curr Protoc Bioinformatics* 54:5.6.1–5.6.37. <https://doi.org/10.1002/cpbi.3>.
 83. Park SY, Borbat PP, Gonzalez-Bonet G, Bhatnagar J, Pollard AM, Freed JH, Bilwes AM, Crane BR. 2006. Reconstruction of the chemotaxis receptor-kinase assembly. *Nat Struct Mol Biol* 13:400–407. <https://doi.org/10.1038/nsmb1085>.
 84. Krivov GG, Shapovalov MV, Dunbrack RL, Jr. 2009. Improved prediction of protein side-chain conformations with SCWRL4. *Proteins* 77:778–795. <https://doi.org/10.1002/prot.22488>.
 85. Krieger E, Joo K, Lee J, Lee J, Raman S, Thompson J, Tyka M, Baker D, Karplus K. 2009. Improving physical realism, stereochemistry, and side-chain accuracy in homology modeling: four approaches that performed well in CASP8. *Proteins* 77(Suppl 9):114–122. <https://doi.org/10.1002/prot.22570>.
 86. Laskowski RA, MacArthur MW, Moss DS, Thornton JM. 1993. PROCHECK: a program to check the stereochemical quality of protein structures. *J Appl Crystallogr* 26:283–291. <https://doi.org/10.1107/S0021889892009944>.
 87. Humphrey W, Dalke A, Schulten K. 1996. VMD: visual molecular dynamics. *J Mol Graph* 14:33–38. [https://doi.org/10.1016/0263-7855\(96\)00018-5](https://doi.org/10.1016/0263-7855(96)00018-5).
 88. Morris GM, Huey R, Lindstrom W, Sanner MF, Belew RK, Goodsell DS, Olson AJ. 2009. AutoDock4 and AutoDockTools4: automated docking with selective receptor flexibility. *J Comput Chem* 30:2785–2791. <https://doi.org/10.1002/jcc.21256>.
 89. Phillips JC, Braun R, Wang W, Gumbart J, Tajkhorshid E, Villa E, Chipot C, Skeel RD, Kale L, Schulten K. 2005. Scalable molecular dynamics with NAMD. *J Comput Chem* 26:1781–1802. <https://doi.org/10.1002/jcc.20289>.
 90. Huang J, MacKerell AD, Jr. 2013. CHARMM36 all-atom additive protein force field: validation based on comparison to NMR data. *J Comput Chem* 34:2135–2145. <https://doi.org/10.1002/jcc.23354>.
 91. Cassidy CK, Himes BA, Sun D, Ma J, Zhao G, Parkinson JS, Stansfeld PJ, Luthey-Schulten Z, Zhang P. 2020. Structure and dynamics of the *E. coli* chemotaxis core signaling complex by cryo-electron tomography and molecular simulations. *Commun Biol* 3:24. <https://doi.org/10.1038/s42003-019-0748-0>.
 92. Walshaw J, Woolfson DN. 2001. Socket: a program for identifying and analysing coiled-coil motifs within protein structures. *J Mol Biol* 307:1427–1450. <https://doi.org/10.1006/jmbi.2001.4545>.
 93. Swain KE, Gonzalez MA, Falke JJ. 2009. Engineered socket study of signaling through a four-helix bundle: evidence for a yin-yang mechanism in the kinase control module of the aspartate receptor. *Biochemistry* 48:9266–9277. <https://doi.org/10.1021/bi901020d>.
 94. Hills EE, Abraham MH, Hersey A, Bevan CD. 2011. Diffusion coefficients in ethanol and in water at 298K: linear free energy relationships. *Fluid Phase Equilib* 303:45–55. <https://doi.org/10.1016/j.fluid.2011.01.002>.
 95. Logg A, Mardal K-A, Wells G (ed). 2012. Automated solution of differential equations by the finite element method. Springer-Verlag, Berlin, Germany.
 96. Geuzaine C, Remacle J-F. 2009. Gmsh: a 3-D finite element mesh generator with built-in pre- and post-processing facilities. *Int J Numer Methods Eng* 79:1309–1331. <https://doi.org/10.1002/nme.2579>.
 97. Ullah AH, Ordal GW. 1981. In vivo and in vitro chemotactic methylation in *Bacillus subtilis*. *J Bacteriol* 145:958–965. <https://doi.org/10.1128/JB.145.2.958-965.1981>.
 98. Kristich CJ, Ordal GW. 2002. *Bacillus subtilis* CheD is a chemoreceptor modification enzyme required for chemotaxis. *J Biol Chem* 277:25356–25362. <https://doi.org/10.1074/jbc.M201334200>.